Ore Geology Reviews 99 (2018) 344–364

Contents lists available at ScienceDirect

Ore Geology Reviews

journal homepage: www.elsevier.com/locate/oregeorev

Platinum-group minerals in the Skouries Cu-Au (Pd, Pt, Te) porphyry deposit

Katie A. McFall[a,b,*], Jonathan Naden[c], Stephen Roberts[b], Tim Baker[d], John Spratt[e], Iain McDonald[a]

[a] School of Earth & Ocean Sciences, Cardiff University, Main Building, Park Place, Cardiff CF10 3AT, UK
[b] Ocean and Earth Science, University of Southampton Waterfront Campus, National Oceanography Centre, European Way, Southampton SO14 3ZH, UK
[c] British Geological Survey, Nicker Hill, Keyworth, Nottingham NG12 5GG, UK
[d] Eldorado Gold Corporation, 1188 Bentall 5-550 Burrard St., Vancouver, British Columbia V6C 2B5, Canada
[e] Core Research Laboratories, Natural History Museum, Cromwell Road, South Kensington, London SW7 5BD, UK

ABSTRACT

The Skouries deposit is a platinum-group element (PGE) enriched Cu-Au porphyry system located in the Chalkidiki peninsula, Greece, with associated Ag, Bi and Te enrichment. The deposit is hosted by multiple porphyritic monzonite and syenite intrusions, which originated from a magma chamber at depth. An initial quartz monzonite porphyritic intrusion contains a quartz–magnetite ± chalcopyrite–pyrite vein stockwork with intense potassic alteration. The quartz monzonite intrusion is cross cut by a set of syenite and mafic porphyry dykes and quartz–chalcopyrite–bornite ± magnetite veins which host the majority of the Cu and Au mineralisation. Late stage quartz–pyrite veins, with associated phyllic alteration crosscut all previous vein generations. Electron microprobe and scanning electron microscopy shows that the PGE are hosted by platinum-group minerals (PGM) in the quartz-chalcopyrite–bornite ± magnetite veins and within potassic alteration assemblages. The PGE mineralisation in Skouries is therefore part of the main high temperature hypogene mineralisation event. Platinum-group minerals at Skouries include: sopcheite [$Ag_4Pd_3Te_4$], merenskyite [(Pd,Pt)$(Te,Bi)_2$] and kotulskite [Pd(Te,Bi)], with rare telargpalite [$(Pd,Ag)_3Te$], isomertieite [$Pd_{11}Sb_2As_2$], naldrettite [Pd_2Sb], testibiopalladite [PdTe(Sb,Te)] and sobolevskite [PdBi]. The most common platinum-group mineral is sopcheite. The PGM in Skouries are small, 52 μm^2 on average, and occur as spherical grains on the boundaries between sulphides and silicates, and as inclusions within hydrothermal quartz and sulphides. These observations support a "semi-metal collector model" whereby an immiscible Bi-Te melt acts as a collector for PGE and other precious metals in high temperature hydrothermal fluids. This mechanism would allow the formation of PGM in porphyries without Pt and Pd fluid saturation.

1. Introduction

Porphyry deposits can contain appreciable amounts of platinum-group elements (PGE), in particular Pt and Pd, with the economic extraction of these valuable by-products of increasing interest (Economou-Eliopoulos, 2010, 2005; Tarkian and Stribrny, 1999). Relatively high (~1 ppm in whole rock) levels of Pd and Pt are described for several porphyries worldwide (Economou-Eliopoulos, 2010). For example, the Elatsite deposit, Bulgaria has an average whole rock Pt content of 16 ppb and Pd content of 40 ppb. Previous studies on Skouries reported Pd contents between 52 and 610 ppb and Pt contents up to 150 ppb in whole rock samples (Augé et al., 2005; Economou-Eliopoulos and Eliopoulos, 2000; Eliopoulos and Economou-Eliopoulos, 1991; Tarkian et al., 2003). Other PGE-enriched porphyries include Santo Tomas II, Philippines; Galore Creek, Lorraine; Mt. Milligan, Mt. Polley & Island Copper, British Columbia; Medet, Bulgaria; Majdanpek, Serbia; Erdenetuin-Obo, Mongolia; Bozshakol, Kazakhstan; Kalmakyr, Uzbekistan; Sora, Aksug, Zhireken and Mikheevskoe, Russia; Mamut, Malaysia and Fengshan, China (Table 1, Augé et al., 2005; Bath et al., 2014; Berzina et al., 2007; Bogdanov et al., 2005; Eliopoulos et al., 2014; Kehayov and Bogdanov, 1987; Lefort et al., 2011; Micko et al., 2014; Pašava et al., 2010; Pass et al., 2014; Plotinskaya et al., 2018; Prichard et al., 2013; Sotnikov et al., 2001; Tarkian et al., 2003; Tarkian and Koopmann, 1995; Tarkian and Stribrny, 1999; Thompson et al., 2001; Wang et al., 2014). Although these PGE-enriched porphyry deposits occur in different geodynamic settings with contrasting ore and

* Corresponding author at: School of Earth & Ocean Sciences, Cardiff University, Main Building, Park Place, Cardiff CF10 3AT, UK.
E-mail address: McFallK@cardiff.ac.uk (K.A. McFall).

https://doi.org/10.1016/j.oregeorev.2018.06.014
Received 10 February 2018; Received in revised form 13 June 2018; Accepted 17 June 2018
Available online 18 June 2018

Table 1
A summary of PGE-enriched porphyries globally showing their common features, Pd and Pt concentrations in whole rock (WR) and concentrate (conc) in ppb (average value in brackets), any platinum group minerals (PGM) present and where they are hosted. The Skouries data is a summary of data from past work, not including that from this study. Blank cells indicate that these features have not yet been classified for that deposit ([a]Augé et al., 2005; [b]Bath et al., 2014; [c]Berzina et al., 2007; [d]Bogdanov et al., 2005; [e]Economou-Eliopoulos and Eliopoulos, 2000; [f]Eliopoulos et al., 2014; [g]Eliopoulos and Economou-Eliopoulos, 1991; [h]Kehayov and Bogdanov, 1987; [i]Lefort et al., 2011; [j]Micko et al., 2014; [k]Pašava et al., 2010; [l]Pass et al., 2014; [m]Plotinskaya et al., 2018; [n]Prichard et al., 2013; [o]Sotnikov et al., 2001; [p]Tarkian et al., 2003; [q]Tarkian and Koopmann, 1995; [r]Tarkian and Stribrny, 1999; [s]Thompson et al., 2001; [t]Wang et al., 2014). BC = British Columbia, bn = bornite, cpy = chalcopyrite, mag = magnetite, PNG = Papua New Guinea. *Copyright (2016) University of Southampton.*

Deposit	Type	Area	Host rock	Pt (WR)	Pt (conc)	Pd (WR)	Pd (conc)	PGM present	PGM hosting
Elatsite[a,d,hp]	AlkalineCu-Au	Bulgaria	Multiphase monzonite	< dl-349 (74)	76	2–3440 (3 7 6)	347	Merenskyite, moncheite	Mag-bn-cpy veins, in cpy and bn
Medet[r]	Calc-alkalineCu-Au	Bulgaria	Granodiorite	< dl-26	8	7–50 (29)	160		
Majdanpek[r]	Calc-alkaline(Cu-Au)	Serbia	Diorite		16–24		52–490	Merenskyite	In cpy
Skouries[e,f,g]	*Shoshonite(Cu-Au)*	*Greece*	*Syenite*	*< dl-150 (30)*	*< 10 – 81 (33)*	*< dl–610 (1 4 9)*	*75 – 2400 (1625)*	*Merenskyite*	*In cpy*
Erdenetuin-Obo[o]	Calc-alkaline(Cu-Mo)	Mongolia	Diorite -granite	< dl-32 (24)	33	7–23 (14)	20		
Santo Tomas II (Philex)[q]	Calc-alkaline(Cu-Au)	Philippines	Quartz diorite	11–38	0.4	22–160	2	Merenskyite, moncheite, kotulskite	Mag-bn-cpy veins, potassic alteration
Bozshakol[o]	Calc-alkaline(Cu-Au-Mo)	Kazakhstan	Tonalite		< dt		245		
Kalmakyr[k]	K-calc-alkaline(Cu-Au-Mo)	Uzbekistan	Monzonite	< dl-11 (6)		2–292 (54)			
Sora[c]	K-calc-alkaline(Cu-Mo)	Russia	Monzodiorite-diorite-syenite	< dl	< dl-110 (88)	9–18 (13)	9–52 (39)		
Aksug[c]	Calc-alkaline(Cu-Mo)	Russia	Diorite-tonalite	17–34 (22)	25–96 (57)	9–31 (16)	17–924 (2 7 2)	Merenskyite	In cpy
Zhireken[c]	K-calc-alkaline(Cu-Mo)	Russia	Diorite-granodiorite	21–37 (28)	299	11–26 (18)	684		
Mamut[r]	Calc-alkaline(Cu-Au)	Malaysia	Adamellite		450–490		1180–1600	Merenskyite, sperrylite	In cpy
Galore Creek[j,s]	Alkaline(Cu-Au)	BC	Trachytes & syenites	15–107 (48)		103–1581 (7 8 3)			
Lorraine[b] ,s	Alkaline(Cu-Au)	BC	Monzonites & syenites	11		19			
Mt Milligan[i,s]	Alkaline(Cu-Au)	BC	Monzonites & syenites	17–111 (48)	111	51–6312	6312	Merenskyite, naldrettite-stibiopalladinite	In Hg-rich pyrites in late stage veins
Mt Polley[l,s]	Alkaline(Cu-Au-Ag)	BC	Monzonite & monzodiorite	7–33 (19)		23–320 (1 4 2)			
Island Copper[s]	Alkaline(Cu-Au)	BC	Monzonite	31–38		63–320			
Fengshan[n,t]	Calc-alkaline(Cu-Mo)	China	Granodiorite		2 – 81 (36)		8 – 32 (22)		
Mikheevskoe[m]	Calc-alkaline(Mo-Cu)	Russia	Diorite & plagiogranite					Merenskyite, sopcheite	In bn-cpy in porphyry-epithermal transition veins

alteration mineralogy, they share some common features (Table 1). For example, they are almost all Cu-Au porphyries with alkaline to calc-alkaline host rocks and they usually contain primary magnetite indicating an oxidised source magma. However, these features are also shared by the majority of Cu-Au porphyry deposits, including those without a known PGE enrichment (e.g. Richards, 2014; Sillitoe, 2010).

Initial studies of the porphyry related PGE mineralisation at Skouries suggested the PGE enrichment was associated with later, shallower and cooler mineralisation phases (Eliopoulos and Economou-Eliopoulos, 1991). However, PGE have been located within the main potassic ore-forming stage in the Elatsite, Santo Tomas II, Kalmakyr, Mamut and Majdanpek deposits. The Elatsite and Santo Tomas II deposits also contain high salinity (> 50 wt% NaCl equivalent) fluid inclusions with high homogenisation temperatures (> 350 °C) in veins associated with PGE enrichment (Kehayov and Bogdanov, 1987; Tarkian and Koopmann, 1995; Tarkian and Stribrny, 1999). These observations suggest that PGE enrichment in porphyries is associated with hypogene ore-forming processes (Economou-Eliopoulos and Eliopoulos, 2000). Fluid inclusions in PGE-bearing veins have high fO_2 (shown by the presence of hydrothermal magnetite), temperature and salinity. These fluid conditions favour the hydrothermal transport of Pd as chloride complexes, and this is currently the accepted mechanism of transport in porphyry deposits (Xiong and Wood, 2000). However, there is also PGE enrichment documented in the later stage porphyry-epithermal transition zone of telescoped deposits such as Mount Milligan and Pagoni Rachi (Lefort et al., 2011; Voudouris et al., 2013), showing that relatively cooler (< 270 °C) vein stages can also be platinum-group mineral (PGM) bearing.

Detailed studies established that at Elatsite the PGE are hosted in merenskyite [(Pd,Pt)(Te,Bi)$_2$], and in a solid solution of merenskyite-moncheite [(Pt,Pd)(Te,Bi)$_2$] which occurs in the main magnetite-chalcopyrite-bornite stage of the deposit. Elatsite also contains other tellurides, including Ag tellurides, bismuthides and selenides, along with a range of Ni-Co sulphides (Augé et al., 2005; Bogdanov et al., 2005; Tarkian et al., 2003). Santo Tomas II hosts its PGE in merenskyite, moncheite and kotulskite [Pd(Te,Bi)] which occur within the main magnetite-bornite-chalcopyrite bearing veins of the potassic core of the deposit. Other semi-metal bearing minerals present include Ag tellurides and selenides (Tarkian and Koopmann, 1995). Additionally stibiopalladinite [Pd_5Sb_2] and vysotskite [(Pd,Ni)S] have been identified in sulphide concentrates from Santo Tomas II (Piestrzynski, 1994), while merenskyite has been identified in sulphide concentrates from Aksug, Majdanpek and Mamut (where sperrylite [$PtAs_2$] was also identified; Tarkian and Stribrny, 1999). A greater variety of PGM have been identified in transitional porphyry-epithermal veins and a range of telluride minerals, including PGM, are often present in alkalic epithermal Au deposits (Lefort et al., 2011; Plotinskaya et al., 2018; Watterson et al., 1977).

In this paper we give a detailed description of the PGE-rich mineralisation in the Skouries deposit, the PGM associations and the host minerals. We discuss the role of semi-metals in PGE enrichment in porphyry deposits, and potential exploration indicators for PGE-enriched porphyry Cu deposits.

1.1. Background regional geology

The Skouries Cu-Au porphyry copper deposit is located on the Chalkidiki Peninsula in north-eastern Greece, 90 km south-east of Thessaloniki (Fig. 1). It is part of the Kassandra mining district (Kroll et al., 2002), in the Serbomacedonian metallogenic province (SMP). The SMP is associated with Late Cretaceous to Tertiary magmatism (Jankovic, 1977), and is a subdivision of the Tethyan Metallogenic Belt, which incorporates all deposits associated with the closure of the Tethyan Ocean (Jankovic, 1997; Richards, 2015). These include the Cretaceous PGE-enriched Elatsite porphyry deposit in Bulgaria (Tarkian et al., 2003), as well as post-collisional deposits such as Skouries (Siron et al., 2016).

The Skouries deposit is situated within the Vertiskos Formation, the upper unit in the Serbomacedonian Massif (Fig. 1, Kroll et al., 2002; Siron et al., 2018). The Vertiskos Formation consists of schists, amphibolite lenses and gneisses which have undergone retrograde metamorphism from amphibolite to greenschist facies (Frei, 1995; Hahn, 2015; Kroll et al., 2002; Siron et al., 2018). It also contains a mafic and ultra-mafic intrusive complex thought to represent a dismembered ophiolite sequence (Dixon and Dimitriadis, 1984; Frei, 1995). The Serbomacedonian Massif is separated from the Rhodope core, a syn-metamorphic Eocene-Miocene metamorphic core complex, by the Kerdilion detachment fault (Brun and Sokoutis, 2007). Exhumation of the Rhodope core complex is closely related to post collisional magmatism and mineralisation (Marchev et al., 2005).

Neogene calc-alkalic magmatism in the region was generated during post-collisional extension by partial melting of subduction-modified lithospheric mantle and crust (Richards 2015; Rosu et al. 2005; Harangi et al. 2007; Harris et al. 2013). The Kassandra mining district consists of several magmatic-hydrothermal ore deposits related to Hellenic subduction and subsequent post-collisional extension (Frei, 1995, 1992; Kroll et al., 2002; Siron et al., 2016). These deposits are associated with two distinct magmatic episodes. One in the late Oligocene (27–25 Ma), and one in the early Miocene (20–19 Ma, Siron et al., 2016), which includes the Skouries porphyry deposit (20.56 ± 0.48 Ma from U-Pb of zircon, Hahn, 2015). These early Miocene alkaline magmatic events are interpreted to be the result of extension following exhumation of the Rhodope core complex (Siron et al., 2016), with magma emplacement triggered by a change in the regional extensional stress field (Siron et al., 2018).

The Miocene magmatism consists of porphyritic stocks and dykes with calc-alkaline to shoshonitic compositions (Kroll et al., 2002; Siron et al., 2016). It also includes regional alkaline porphyry dykes, locally described as “black matrix porphyry dykes” because of their dark aphanitic groundmass in hand specimen. These were originally classified as lamprophyres (e.g. Kalogeropoulos et al., 1989), however a recent study has shown them to have a trachy-andesitic composition (Siron et al, 2016). They have been suggested as a potential metal source for the Skouries deposit as they are very close in age, and similar units are present within the deposit (Eliopoulos et al., 2014; Siron et al., 2016).

Skouries has a measured and indicated resource of 289 million tonnes at 0.58 g/t Au and 0.43% Cu for 5.4 Moz Au and 1.2 Mt Cu (Eldorado Gold Corp, 2017). Potassic alteration and copper mineralisation, including veining, extend into the surrounding country rock with approximately two thirds of the measured and indicated ore reserves hosted outside the porphyry (Eldorado Gold Corp, 2017).

2. Deposit geology

The Skouries deposit is hosted in a pipe shaped system 200 m in diameter, exceeding 900 m in depth, which consists of several generations of porphyritic intrusions of monzonitic to syenitic composition (Fig. 2). Intense potassic alteration commonly obscures the original mineralogy. Detailed logging of 3465 m of drill core from five drill holes reveals four porphyritic phases: The first phase is an early quartz monzonite containing 40–55% remnant plagioclase feldspar phenocrysts, along with 5–20% primary anhedral biotite phenocrysts 1–2 mm in diameter and 5–10% anhedral quartz phenocrysts 2–5 mm in diameter in an aphanitic matrix. This unit has undergone extensive potassic alteration, with the groundmass and a large proportion of the phenocrysts altered to potassium feldspar. This unit is crosscut by intense early stage veining (Fig. 3a).

The second phase is a syn-mineralisation porphyritic syenite unit which cross-cuts both the initial monzonite, and the early stage veining. The syenite contains 60% anhedral-subhedral feldspar phenocrysts, 5–10% (< 1 mm) anhedral primary biotite and ~2% subhedral

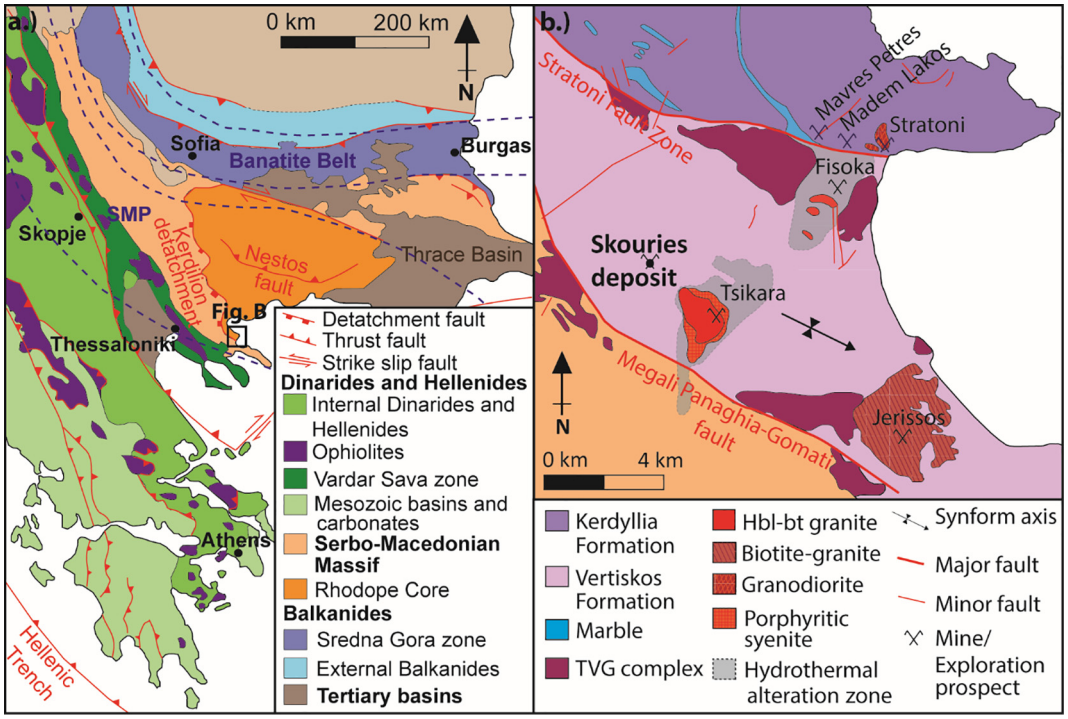

Fig. 1. a.) Regional geology map showing the major tectono-stratigraphic units, metallogenic belts and major structural features of the area surrounding the Skouries deposit (modified from Hahn 2015 and Burg 2012 incorporating data from Frei 1995). b.) Local geology map of the region around Skouries (inset in a) showing the geological units, major structures and regional mines and exploration prospects (after Kroll et al. 2002; Frei 1995; Eliopoulos and Economou-Eliopoulos 1991; Eldorado Gold Corp, 2017).

(1–2 mm) amphibole (Fig. 3a). These are hosted in a potassium feldspar aphanitic groundmass containing disseminated magnetite. The unit contains rare unaltered plagioclase feldspar phenocrysts, along with potassium feldspar megacrysts 1–4 cm in diameter. At shallow depths this syenite is crosscut by a fine-grained unit with the same mineralogy. However, below depths of > 600 m the two units show mixing textures, with no clear boundaries between the two, suggesting they are the same unit.

The third intrusive phase is represented by a series of porphyritic mela-syenite dykes which cross-cut and are cross-cut by the syn-

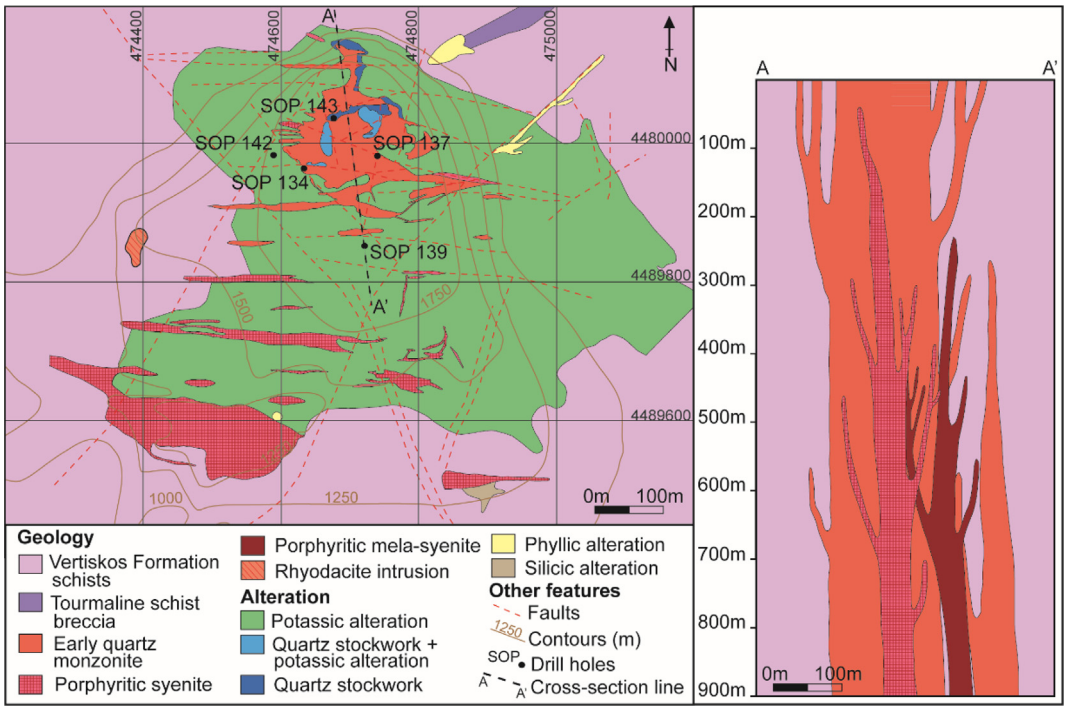

Fig. 2. Geological map and schematic cross section of Skouries. Geological map modified from TVX Hellas, schematic cross section adapted from Kroll et al (2002) using logging performed in this study. The drill holes shown are the ones logged in this study. Map with borehole locations reproduced with permission of Eldorado Gold Corporation, Vancouver, Canada.

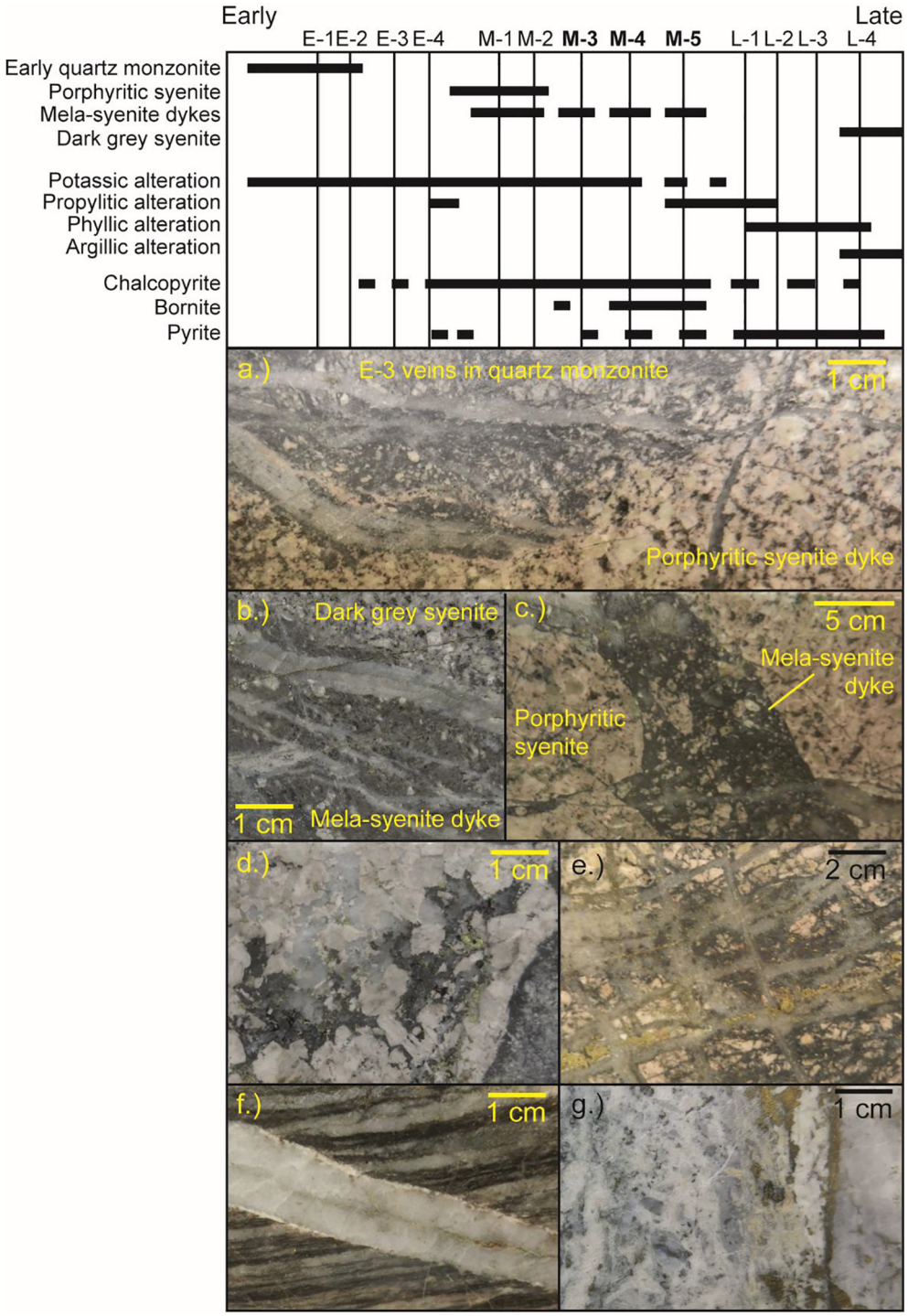

Fig. 3. Paragenesis of the Skouries deposit showing the relative timing of the host intrusions, alteration stages, sulphides and vein stages. Veins associated with Cu-Au mineralisation are in bold. Photographs from core of: a.) Dense network of early stage (E-1 and E-3) veins in quartz monzonite being cross-cut by the porphyritic syenite unit and M − 2 veins. b.) Mela-syenite dyke with M − 2 and M − 5 veins cross-cut by post-mineralisation dark grey syenite c.) Mela-syenite dyke cross-cutting and brecciating porphyritic syenite and M − 5 vein d.) Alteration selvage at the edge of a M − 3 vein with large secondary orthoclase and biotite crystals. e.) M − 4 vein stockwork f.) M − 5 vein in biotite schist country rock. g.) L-4 polymetallic quartz-barite vein. *Copyright (2016) University of Southampton.*

mineralisation syenite and brecciate the earlier units (Fig. 3b, c). This intrusive phase consists of 5–20% subhedral to euhedral K-spar phenocrysts (2–3 mm); 5–10% biotite subhedral phenocrysts (1 mm), 3% euhedral amphibole phenocrysts (1 mm) and 1% disseminated magnetite (< 1 mm) in an aphanitic dark grey groundmass. These dykes are similar in appearance and composition to the regional alkaline "black matrix porphyry dykes" described above. The porphyritic syenite and mela-syenite dykes are associated with main stage vein sets which host the majority of the Cu and Au mineralisation. These vein sets and igneous units are crosscut by the fourth igneous phase, a later dark grey porphyritic syenite which does not host any mineralisation (Fig. 3b).

2.1. Alteration and mineralogy

The Skouries deposit is a small (< 400 m in diameter) vertical, pipe-like body of quartz-sulphide vein stockwork mineralisation centred on the host porphyry stock. Based on crosscutting and overprinting relationships 14 stages of veining and associated alteration have been identified (Table 2). These have been classified into three groups: early (E) stage, associated with the initial quartz monzonite porphyritic phase; main (M) stage, associated with the *syn*-mineralisation porphyritic syenite and the porphyritic mela-syenite dykes; and the late (L) stage which crosscuts all earlier phases and is associated with low temperature alteration assemblages (Fig. 3).

Table 2
Description of the main vein stages in the Skouries deposit from core logging performed during this study (*syn*-min = *syn*-mineralisation). *Copyright (2016) University of Southampton.*

Vein stage	Vein Type	Associated Igneous Phases	Description	Associated Alteration	Associated mineralisation
E-1	Biotite-magnetite	Early monzonite	Wavy biotite-magnetite veinlets, 1–2 mm thick, aligned	Orthoclase, biotite, magnetite	
E-2	Quartz	Early monzonite	Wavy quartz veinlets 2 – 10 mm thick, regular anhedral quartz crystals.	Orthoclase, biotite, magnetite	
E-3	Quartz-magnetite + /-chalcopyrite	Early monzonite	Wavy, structurally aligned stockwork of 8 – 20 mm thick quartz veins with magnetite along the margins and disseminated in the centre, sometimes with minor chalcopyrite.	Magnetite, biotite	Minor chalcopyrite
E-4	Sulphide - chalcopyrite/pyrite	Early monzonite	Wavy sulphide veinlet 1–3 mm thick	Magnetite, biotite	Chalcopyrite-pyrite
M – 1A	Biotite-magnetite	Syn-min syenite	Wavy biotite-magnetite veinlets, 2–5 mm thick	Orthoclase, biotite, magnetite	
M – 1B	Hydrothermal orthoclase	Syn-min syenite	Irregular hydrothermal orthoclase veinlets 5 mm to 10 cm thick		
M – 2	Quartz	Syn-min syenite	Wavy quartz veinlets 2–4 mm thick, regular anhedral quartz crystals.	Orthoclase, often altered to sericite	
M – 3	Quartz-biotite-orthoclase-chalcopyrite + /-magnetite	Syn-min syenite	Curvilinear quartz veins 8–40 mm wide with euhedral potassium feldspar and secondary biotite selvage. Often with massive sulphides in the centre of the vein, intergrown with quartz crystals. Large euhedral quartz crystals.	Secondary biotite, potassium feldspar	Chalcopyrite (bornite, pyrite)
M – 4	Quartz-magnetite-bornite-chalcopyrite	Syn-min syenite	Straight veins 1–5 cm wide with small anhedral quartz crystals containing trails of sulphides and magnetite parallel to vein edges. Often form stockworks.	Potassium feldspar, magnetite, secondary biotite, sericite	Bornite, chalcopyrite
M – 5	Quartz-chalcopyrite-bornite veins	Syn-min syenite	Straight quartz veins 1–3 cm wide, containing sulphides in a central suture, with small, regular, subhedral crystals.	Potassium feldspar in selvage, biotite and chlorite	Chalcopyrite, bornite, pyrite
L-1	Gypsum	Syn-min syenite	Wavy gypsum veinlets 4–8 mm thick	Phyllic alteration, disseminated hematite	
L-2	Sulphide	Syn-min syenite	Wavy pyrite veinlet 2–10 mm thick	Sericite, pyrophyllite	Pyrite
L-3	Quartz-calcite	Syn-min syenite	Straight quartz veins 8–15 mm with calcite-sericite in a central suture, cloudy white quartz	Sericite, clay	
L-4	Quartz-barite-sulphide	Syn-min syenite	Large quartz-barite veins (5–15 cm) with large euhedral 'comb' morphology quartz crystals interlocking with barite. Contain large irregular masses of sulphides. Occasionally contains apatite.	Calcite, dolomite, sericite, clay	Pyrite, sphalerite, galena

The deposit has pervasive, potassic alteration which has destroyed the original textures and mineralogy (Fig. 4). The large propylitic and phyllic alteration zones commonly found in other porphyries are not present in Skouries. Propylitic alteration is present as an irregular and patchy overprint in a narrow halo around the intrusions, while the later phyllic alteration is only associated with faults and fractures in the deposit. The different alteration phases of the deposit are described in more detail in relation to their associated vein stages below.

2.1.1. *Early stage vein sets*

Early stage veins (E-1 – E-4; Table 2) are characterised by abundant magnetite and have indistinct, wavy margins suggesting they formed at temperatures consistent with ductile deformation (Fig. 3a). They are associated with pervasive potassic alteration assemblages of orthoclase-biotite-magnetite. These alteration minerals replace primary feldspar, amphibole and biotite phenocrysts, and are also present as disseminated aggregates of biotite–magnetite 1–2 mm across (Fig. 4). The groundmass of the host quartz monzonite is commonly completely altered to orthoclase in areas with a high proportion of early veining (Fig. 3a).

The E-1 vein stage contains orthoclase–biotite–magnetite and consists of wavy to sinuous magnetite-biotite veinlets 1–2 mm across. E-2 veins consist of wavy to sinuous quartz veinlets 2–10 mm across, containing regular anhedral quartz crystals. These veins commonly branch and cross-cut each other and have large secondary orthoclase and biotite phenocrysts overgrowing them.

E-3 veins contain quartz–magnetite ± chalcopyrite. They consist of a wavy, structurally aligned stockwork of quartz veins 8–20 mm across, with magnetite along the margins and disseminated in the centre. Occasionally they also contain minor chalcopyrite disseminated within the vein quartz. They truncate E-1 and E-2 veins and are interpreted to have formed in a semi-ductile regime. The E-3 veins are associated with disseminated magnetite and biotite alteration. The final early stage veins, E-4 veins, contain chalcopyrite-pyrite, and consist of wavy to sinuous sulphide veinlets 1–3 mm across. These crosscut E-1 to E-3 and are often accompanied by a fine-grained magnetite-biotite alteration selvage. These early vein sets, particularly E-3, are also present in the surrounding Vertiskos Formation gneisses and schists.

2.1.2. *Main stage vein sets*

The main stage vein sets (M − 1 – M − 5) are characterised by a potassic alteration assemblage consisting of orthoclase, biotite and magnetite; as well as the presence of bornite and chalcopyrite. They are associated with the *syn*-mineralisation porphyritic syenite and the porphyritic mela-syenite dykes, both of which cross-cut the early veins (Fig. 3a, b). Pervasive orthoclase alteration of the groundmass of the *syn*-mineralisation porphyritic syenite occurs with main stage veining. This is accompanied by secondary biotite and magnetite alteration of the biotite and amphibole phenocrysts in both this unit and the porphyritic mela-syenite dykes. Main stage veining is also associated with disseminated magnetite alteration envelopes, commonly with chalcopyrite and bornite also disseminated with the magnetite (Fig. 4c, f, i, l).

The M − 1 vein set contains hydrothermal biotite–magnetite–orthoclase. Two generations of M − 1 structures occur: M − 1A consists of sinuous biotite–magnetite veinlets 2–5 mm in width, while M − 1B consists of irregular hydrothermal orthoclase veinlets 5 mm–10 cm wide which commonly broaden to flood an area, creating large irregular patches of hydrothermal orthoclase. M − 1A veins are distinct from E-1 veins as they truncate E-2 veins, and crosscut E-1 and E-3 veins; however they are truncated by M − 1B veins. M − 2 veins consist of wavy, irregular quartz veinlets 2–4 mm which crosscut the early vein sets (Fig. 3a, b) with a fine-grained orthoclase alteration envelope 1–2 mm wide, which is sometimes altered to sericite.

There are 3 main stage vein sets which are associated with the majority of the Cu-Au mineralisation in the deposit: M − 3, M − 4 and M − 5. The M − 3 vein set contains biotite, orthoclase, quartz and

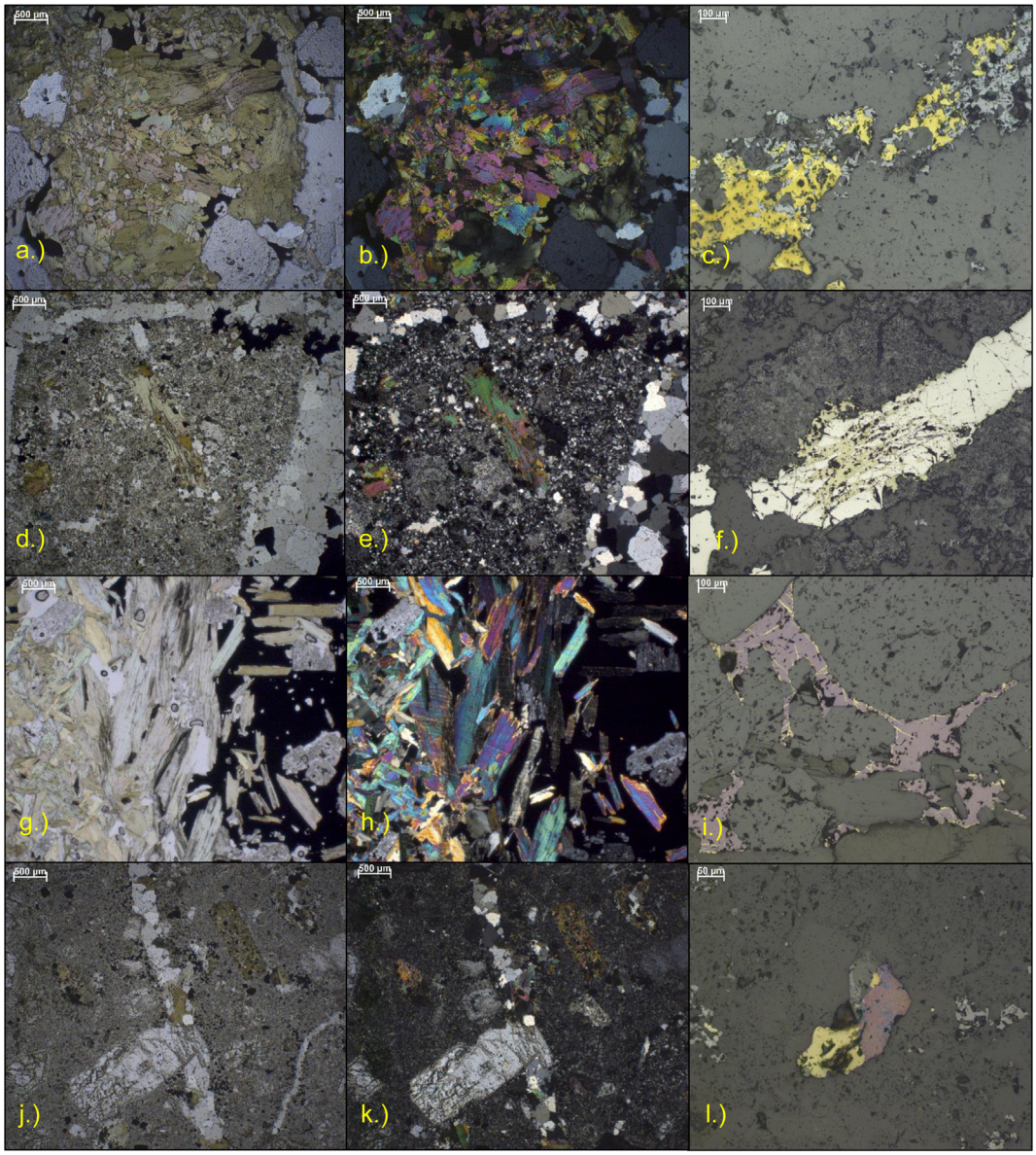

Fig. 4. Photomicrographs of the main alteration and mineralisation stages of Skouries: a.) PPL and b.) XPL photomicrograph of biotite alteration on the edge of an M − 4 vein, with a chlorite overprint. c.) Chalcopyrite and magnetite in M − 4 vein. d.) PPL and e.) XPL photomicrograph of secondary biotite altering a primary biotite phenocryst, and potassium feldspar replacing primary plagioclase phenocrysts in an altered feldspar groundmass. f.) Chalcopyrite filling cracks in pyrite in M − 5 vein. g.) PPL and h.) XPL photomicrograph of euhedral hydrothermal biotite crystals and potassium feldspar phenocrysts at edge of massive chalcopyrite in an M − 3 vein. i.) Chalcopyrite infilling cracks in bornite in M − 4 vein. j.) PPL and k.) XPL photomicrograph of altered biotite and feldspar phenocrysts in an altered groundmass, crosscut by an E-2 quartz vein. The vein is overgrown by secondary hydrothermal potassium feldspar and biotite crystals. l.) Chalcopyrite, bornite and magnetite in an M − 4 vein. *Copyright (2016) University of Southampton.*

chalcopyrite ± magnetite, with minor bornite. These are wavy, discontinuous and curvilinear quartz veins 8–40 mm wide, with a 5–20 mm wide interlocking potassium feldspar and secondary biotite selvage (Figs. 3b, 4g, h). The crystals of quartz, orthoclase and biotite are euhedral and > 6 mm, with embayments and large crystals of biotite and orthoclase within the vein. M − 3 veins have massive chalcopyrite in the centre. This chalcopyrite is 3–30 mm in width, and commonly encloses euhedral quartz crystals towards the edges of the sulphide, rarely with biotite and orthoclase crystal inclusions. Smaller (5–10 mm thick) M − 3 veins contain trails of sulphide crystals, including rare bornite, late pyrite and minor galena on the edges of chalcopyrite crystals.

Vein set M − 4 contains magnetite, quartz, bornite and chalcopyrite. It consists of veins with sinuous to straight margins 10–50 mm wide, with anhedral quartz crystals, containing trails of chalcopyrite-bornite and magnetite parallel to vein edges. These commonly have an orthoclase selvage 5–10 mm wide, are accompanied by a disseminated magnetite alteration envelope and often form stockworks (Figs. 3c, 4a, b). M − 4 veins contain more bornite than chalcopyrite, with chalcopyrite commonly forming a secondary phase in fractures within bornite (Fig. 4i, l). Minor galena is also present on the edge of chalcopyrite crystals.

The M − 5 stage veins consist of straight, planar quartz veins 1–3 cm wide, containing sulphides in a linear central suture, with small, regular, subhedral crystals (Fig. 3b, c, d). The sulphides present are pyrite-chalcopyrite-bornite with minor galena rimming sulphide assemblages (Fig. 4f). The earliest phase is pyrite and, unlike the M − 4 veins, M − 5 veins contain more chalcopyrite than bornite, with the chalcopyrite and bornite co-precipitated. They are associated with biotite-orthoclase-chlorite alteration and commonly have an orthoclase selvage 5 mm

Table 3
Samples analysed for PGM (Syn-min = *syn*-mineralisation). Pd, Pt, Cu and Au concentrations are from commercial assay performed at AcmeLabs and reproduced with permission of Eldorado Gold Corporation, Vancouver, Canada. *Copyright (2016) University of Southampton.*

Sample	Drill hole	Depth (m)	Lithology	Alteration	Veins present	Sulphides present	Pd assay value (ppb)	Pt assay value (ppb)	Au assay value (ppb)	Cu assay value (ppm)
1	137	733	Syn-min syenite	Potassic	M − 3	Pyrite, chalcopyrite	52	2	1137	9269
3	134	261	Syn-min syenite	Potassic, chlorite & sericite	M − 5	Pyrite, chalcopyrite, bornite	139	2	328	1900
4	134	135.1	Syn-min syenite	Potassic	M − 3	Pyrite, chalcopyrite	20	1	497	2958
6	139	521.7	Early monzonite	Potassic	M − 5	Chalcopyrite, pyrite	529	12	1133	4113
8	137	133.9	Syn-min syenite	Potassic	M − 3	Chalcopyrite,	189	6	15,200	145,450
9	139	655	Early monzonite	Potassic & clay	M − 4	Chalcopyrite	393	6	313	1693
11	137	419.5	Early monzonite	Potassic	M − 5	Chalcopyrite, pyrite	126	3	1024	5487
13	134	634.6	Syn-min syenite	Potassic	M − 3	Chalcopyrite, pyrite, bornite	128	4	534	3898
26	134	266.1	Syn-min syenite	Potassic	M − 3	Pyrite, chalcopyrite, bornite	36	1	1516	12,280
31	139	514	Early monzonite	Potassic & clay	M − 4	Chalcopyrite, bornite	1051	11	1473	10,650
34	139	497.6	Early monzonite	Potassic & clay	M − 4 & M − 5	Chalcopyrite, bornite	330	7	1825	8022
36	137	128.1	Syn-min syenite	Potassic & clay	M − 3	Chalcopyrite	728	12	606	3413

wide. Secondary biotite alteration around M − 5 veins commonly shows regression to chlorite, and the M − 5 veins are commonly associated with minor specular hematite, barite, anhydrite and sericite, and very rare epidote.

2.1.3. Late stage vein sets

The late stage (L1 – L4) veins in the Skouries deposit are associated with phyllic alteration assemblages. Alteration minerals present include sericite, quartz, calcite and dolomite, with minor advanced argillic assemblages of kaolinite and pyrophyllite (Fig. 3e). Argillic alteration minerals are also found around cm-scale fractures and metre-scale joints which are present locally in the deposit. l-1 stage veins consist of wavy gypsum veinlets 4–8 mm thick. These are present in areas with phyllic alteration and are associated with disseminated hematite. l-2 stage veins are wavy to sinuous pyrite veinlets 2–10 mm thick with a sericite-pyrophyllite alteration selvage. These veins develop within fractures and crosscut most lithologies and vein sets. l-3 veins consist of straight sided quartz veins 8–15 mm wide with calcite-sericite in a central suture and a sericite-clay alteration selvage. They are rare and are found in fractures. l-4 veins are irregular quartz-barite veins 5–15 cm thick with large euhedral comb morphology quartz crystals on the outer edges of veins. The centre of L-4 veins consist of white fine-grained quartz interlocked with barite crystals (Fig. 3g). These veins contain irregular masses of pyrite-sphalerite-galena, usually only in the fine grained central section, and occasionally contain apatite. They are surrounded by a calcite-dolomite-sericite-clay alteration envelope and are present in vicinities with intense fracturing, usually aligned with the fractures.

2.1.4. Vein densities and mineralisation

Vein densities in Skouries range from 74% (by surface area of bisected core) in the most altered areas to 3.5% in the least altered areas. The vein type with the highest density are the E-3 veins, which commonly show vein densities of > 45%. The mineralising vein sets, M − 3, M − 4 and M − 5 show vein densities of 3.5–11%, with a mean vein density of ~5%. Of these, M − 5 veins are the most sparse, rarely occurring in densities > 4%, while M − 4 veins form stockworks of up to 11% of total core area and M − 3 veins account for up to 10% of the core area in the sections where they occur, although this is mainly due to their variable thickness (up to 4 cm), rather than increased numbers of veins in one section. Vein density is greatest in the core of the deposit, with drill holes logged within the country rock showing significantly lower vein densities of < 5%. M − 3 veins are only present within the core of the deposit, whereas M − 4 and M − 5 veins are both present within the surrounding country rock.

The Cu-Au mineralisation is associated with the main stage veins, particularly M − 3, M − 4 and M − 5, and in disseminated chalcopyrite and bornite in the potassic alteration associated with these vein sets. The Cu in the deposit is primarily hosted in chalcopyrite and bornite, although there is a near-surface oxidation horizon containing malachite and azurite. Other copper secondaries such as covellite and chalcocite are also present down to approximately 60 m below the surface. The Au in the deposit is mainly hosted in electrum, which is an accessory mineral in potassic alteration and in M − 3, M − 4 and M − 5 veins, with native gold also present in M − 4 and M − 5 veins. The deportment of Au, Ag and PGE is discussed further below.

3. Samples and methods

Logging was carried out on 3465 m of drill core across five drill holes in the centre of the deposit (Fig. 2). The visual estimates of vein density made during logging were recorded as a % of the visible surface area in bisected core for each 2 m logging interval. These initial estimates were then validated using the Image-J ™ software package and photographic images of core sections in order to calculate the error of the previously acquired visual estimations. This approach showed that

the visual estimates were accurate to within 10% in high vein density areas, with a tendency to over-estimate vein density, and to within 3% in low vein density areas.

Drill core samples were then selected for analysis based on palladium and platinum concentrations from company assay data provided by Eldorado Gold Corporation, and on the core logging performed during this study. The company whole rock assay analyses were performed at AcmeLab (Bureau Veritas) with Au analysed for by fire assay and all other elements (including Pd and Pt) analysed by ultratrace multi-element ICP-MS after Aqua Regia digest.

Polished thin sections were prepared and examined for visible platinum-group minerals using reflective light microscopy. As the platinum-group minerals are mainly < 20 μm in diameter they were difficult to identify through optical microscopy, so the 12 samples with the highest assay values (Table 3) were selected for further analysis using scanning electron microscopy (SEM) with energy-dispersive X-ray spectroscopy (EDS), and electron probe microanalysis (EPMA) using wavelength dispersive X-ray spectrometry (WDS). Samples from the early and late vein sets were also analysed on the SEM in order to provide non PGE-enriched comparators.

Platinum-group minerals (PGM) were characterised at the National Oceanography Centre, University of Southampton using a LEO1450VP SEM, coupled to an Oxford Instruments X-Act EDS detector. Further characterisation was carried out at Cardiff University using a Zeiss Sigma HD Field Emission Gun Analytical SEM (A-SEM) coupled to two Oxford Instruments EDS detectors and an Oxford Instruments WDS detector. Non-standardised EDS was used for first pass mineral identification and semi-quantitative analysis using spectrum indexes from the AZtec software package (Tables A.1 and A.2), with WDS analysis used to check the stoichiometry of minerals. The area of each PGM was measured from back-scattered electron images using the Image-J™ software package. All relative proportions of mineral phases discussed use area, rather than number of grains identified.

EPMA-WDS was used to confirm the minerals present and to gain quantitative major and trace element data for 23 minerals in six samples (those with the most platinum-group minerals). A Cameca SX100 WDX electron microprobe, at the Natural History Museum (NHM), was used to gain trace element data for minerals containing the PGE and Au. The minerals were located using co-ordinates relative to a reference point acquired on the SEM. A beam current of 20nA, an accelerating voltage of 20 keV and a spot size of 1 μm were used to determine the following elements: S (Kα), Pt (Lα), Mn (Kα), Fe (Kα), Co (Kα), Ni (Kα), Cu (Kα), Zn (Kα), As (Lα), Se (Lα), Pd (Lα), Ag (Lα), Sb (Lα), Te (Lα), Pb (Mα), Bi (Mβ), Cr (Kα), Ru (Lα), Rh (Lα), Os (Mα), Ir (Lα), Au (Lα) and Si (Kα). Standards used were BiTe, Pb_3Se and pure metal for the other elements. Major peak overlaps were performed prior to matrix correction. A small number of minor empirical corrections obtained from standard data were applied to compensate for small peak overlaps. QA was performed on the NHM's in-house standard, with accuracy and precision data given in Table A.1. Accuracy and precision are defined as excellent for all elements (Piercey, 2014). Only the six PGM with an analytical total of 100 ± 3 are presented, with the rest of the data treated as semi-quantitative. The SEM-EDS data from the Cardiff University A-SEM was found to be within 2 wt% of the EPMA-WDS data from the Natural History Museum for the same PGM (Tables 4, Table A.1) and so although the SEM-EDS data is still treated as semi-quantitative, PGM classifications were also obtained using this method.

4. Results

4.1. Platinum-group mineral identification

A total of 45 platinum-group mineral grains (PGM) were identified in 12 polished thin sections. Each mineral grain was classified by compositional type, texture and mineral associations. A list of PGM identified using semi-quantitative EDS and SEM-WDS are presented in Table 4, along with their host mineral and texture (Fig. 5; Table A.2). The PGM are small, with an average surface area of 52 μm^2, and a range of 1.7–1088 μm^2. EPMA-WDS data showing the exact element proportions and confirming the mineral classification of six PGM are presented in Table 5.

There are PGM present in vein sets M − 3, M − 4 and M − 5, with none identified in any of the other vein sets. 20% of the PGM identified were found in M − 3, 6% in M − 4 and 74% in vein set M − 5 (Fig. 6a). The PGM were classified by their textural association: enclosed in sulphide (Figs. 5c, e, f, 5i, 5j, 5 k), enclosed in a hydrothermal alteration silicate mineral (Fig. 5a, h, l) or on a sulphide-silicate boundary (Figs. 5b, d, k, 6c). 18% of the PGM identified are enclosed in sulphides, most commonly chalcopyrite or bornite in the centre of veins, and this textural association is most common in vein set M − 3. 15% of the PGM identified are enclosed in hydrothermal silicate minerals, most commonly within euhedral quartz crystals in the main body of the veins (Fig. 5l). Some are also enclosed in secondary biotite or potassium feldspar in the alteration selvage of the veins (Fig. 5a), and this is most common in vein set M − 5. 67% of the PGM are on the boundary between sulphide and hydrothermal quartz in the centre of the vein sets, most commonly in vein set M − 5. The PGM fall into two morphological classifications – 79% of the PGM have spherical or oblate rounded morphology (Fig. 5a–c, e, f, i, k, l) and 21% have angular morphology (Fig. 5d, g, h, j). Those enclosed in sulphides and hydrothermal silicate minerals are always rounded, with those on crystal boundaries showing both rounded and angular morphologies, with rare PGM filling fractures in sulphides (Fig. 5g).

All the PGM identified were Pd minerals with only very minor Pt concentrations (up to 3 wt% Pt in three merenskyites), and EPMA-WDS shows only trace amounts (< 1 wt%) of Rh and Os to be present in some PGM. No Ru or Ir was detected in any of the PGM analysed. EPMA-WDS data confirms the presence of sobolevskite, sopcheite, testibiopalladite and merenskyite (Table 5). Of all 23 platinum-group minerals analysed using EPMA-WDS, including those with analytical totals outside the 100 + /-3 wt% range, nine are sopcheite, five are sobolevskite, three are merenskyite, two are kotulskite and one is testibiopalladite, with three minerals which had too much background interference to determine composition.

The PGM identified using both EPMA-WDS and SEM-EDS are grouped as Pd bismuth-tellurides, Pd bismuthides, Pd tellurides, Pd-Ag tellurides, and Pd antimonides. 77% of the PGM identified are Pd-Ag tellurides, consisting of sopcheite [$Ag_4Pd_3Te_4$] and rare telargpalite [$(Pd,Ag)_3Te$]. Sopcheite is present in vein sets M − 3, M − 4 and M − 5, with the largest area present in vein set M − 5 (Fig. 6a). 16% of the PGM identified are Pd bismuth-tellurides, predominately merenskyite [$(Pd,Pt)(Te,Bi)_2$] and kotulskite [Pd(Te,Bi)]. These are also present in M − 3, M − 4 and M − 5, with M − 3 having the largest proportion and M − 5 the lowest (Fig. 6a). The merenskyites and kotulskites are Bi-rich rather than Te-rich (Fig. 6b). 5% of the PGM are Pd antimonides, consisting of testibiopalladite [PdTe(Sb,Te)], isomertieite [$Pd_{11}Sb_2As_2$] and naldrettite [Pd_2Sb], and 2% of the PGM are Pd bismuthides, commonly sobolevskite [PdBi], all of which are only present in vein set M − 5.

The samples also contain rounded inclusions of Bi-Te minerals in hydrothermal quartz, chalcopyrite and bornite crystals. These are commonly < 10 μm^2 and so are difficult to analyse with SEM-EDS/EPMA-WDS without interference from surrounding minerals, however they appear to have compositions between those of pilsenite [Bi_4Te_3] and tsumoite [BiTe]. This may be due to intergrowths between members of the tetradymite group at nanoscale (Ciobanu et al., 2009; Cook et al., 2007).

4.2. Other precious metal-bearing minerals

A total of 59 grains of other precious metal (Au and Ag with no PGE) bearing minerals were identified (Tables 6, 7, A.3; Figs. 5, 6). EPMA

Table 4
Platinum group minerals identified in the Skouries deposit (using SEM-EDS and SEM-WDS). HT silicate = hydrothermal alteration silicate mineral, Kspar = potassium feldspar.*Copyright (2016) University of Southampton.*

Sample	Vein set	Mineral	Host	Size (μm^2)	Texture	Host type	PGM type
3	M−5	Sobolevskite	Bornite	32	Angular	Edge of sulphide	PdBi
3	M−5	Sobolevskite	Bornite	9	Rounded	In sulphide	PdBi
3	M−5	Sopcheite	Bornite	6	Angular	In sulphide	PdBi
3	M−5	Sopcheite	Chalcopyrite	31	Rounded	Edge of sulphide	PdAgTe
3	M−5	Sopcheite	Kspar	4	Rounded	Edge of sulphide	PdAgTe
6	M−3	Kotulskite	Quartz	6	Spherical	In HT silicate	PdBiTe
6	M−3	Merenskyite	Chalcopyrite	10	Spherical	In sulphide	PdBiTe
6	M−3	Sopcheite	Chalcopyrite	14	Spherical	Edge of sulphide	PdAgTe
8	M−3	Kotulskite	Quartz	4	Spherical	In HT silicate	PdBiTe
9	M−3	Merenskyite	Chalcopyrite	20	Spherical	Edge of sulphide	PdBiTe
9	M−3	Sopcheite	Quartz	50	Spherical	In HT silicate	PdBiTe
9	M−3	Sopcheite	Chalcopyrite	131	Spherical	Edge of sulphide	PdAgTe
9	M−3	Sopcheite	Quartz	68	Spherical	In HT silicate	PdAgTe
11	M−5	Isomertieite (?)	Chalcopyrite	65	Angular	Edge of sulphide	PdSb
11	M−5	Kotulskite	Quartz	8	Spherical	In HT silicate	PdBiTe
11	M−5	Naldrettite (?)	Chalcopyrite	23	Rounded	In sulphide	PdSb
11	M−5	Sopcheite	Chalcopyrite	14	Angular	In sulphide	PdAgTe
11	M−5	Sopcheite	Chalcopyrite	1088	Rounded	Edge of sulphide	PdAgTe
11	M−5	Sopcheite	Quartz	190	Angular	In HT silicate	PdAgTe
26	M−3	Sopcheite	Chalcopyrite	5	Angular	Edge of sulphide	PdAgTe
31	M−4	Kotulskite	Quartz	5	Spherical	In HT silicate	PdBiTe
31	M−4	Merenskyite	Chalcopyrite	50	Angular	In sulphide	PdBiTe
31	M−4	Sopcheite	Chalcopyrite	32	Spherical	In sulphide	PdAgTe
31	M−4	Sopcheite	Quartz	50	Angular	Edge of sulphide	PdAgTe
31	M−4	Sopcheite	Quartz	5	Spherical	In HT silicate	PdAgTe
31	M−4	Telargpalite	Chalcopyrite	5	Angular	In sulphide	PdAgTe
34	M−5	Kotulskite	Chalcopyrite	5	Spherical	In sulphide	PdBiTe
34	M−5	Kotulskite	Clay	15.2	Spherical	In HT silicate	PdBiTe
34	M−5	Merenskyite	Quartz	6	Spherical	In HT silicate	PdBiTe
34	M−5	Merenskyite	Chalcopyrite	18	Spherical	In sulphide	PdBiTe
34	M−5	Merenskyite	Chalcopyrite	32	Spherical	In sulphide	PdBiTe
34	M−5	Merenskyite	Quartz	42	Rounded	Edge of sulphide	PdBiTe
34	M−5	Sopcheite	Biotite	28	Rounded	Edge of sulphide	PdAgTe
34	M−5	Sopcheite	Chalcopyrite	10	Spherical	In sulphide	PdAgTe
34	M−5	Sopcheite	Kspar	20	Spherical	Edge of sulphide	PdAgTe
34	M−5	Sopcheite	Kspar	1.7	Spherical	In HT silicate	PdAgTe
34	M−5	Sopcheite	Magnetite	17	Angular	Edge of sulphide	PdAgTe
34	M−5	Testibiopalladite	Bornite	38	Spherical	In sulphide	PdTe
36	M−3	Merenskyite	Chalcopyrite	47	Angular	In sulphide	PdBiTe
36	M−3	Merenskyite	Chalcopyrite	27	Spherical	In sulphide	PdBiTe
36	M−3	Merenskyite	Chalcopyrite	3	Spherical	In sulphide	PdBiTe
36	M−3	Merenskyite	Chalcopyrite	56	Spherical	In sulphide	PdBiTe
36	M−3	Merenskyite	Chalcopyrite	12	Rounded	In sulphide	PdBiTe
36	M−3	Sopcheite	Chalcopyrite	4	Angular	In sulphide	PdAgTe
36	M−3	Sopcheite	Chalcopyrite	17	Spherical	In sulphide	PdAgTe

analysis confirmed the presence of electrum [AgAu], hessite [Ag_2Te] and rare stützite [Ag_5-xTe_3, (x = 0.24–0.36)] (Table 7). SEM-EDS and SEM-WDS analysis also shows the presence of empressite [AgTe], muthmannite [$AgAuTe_2$], sylvanite [$(Au,Ag)_2Te_4$], volynskite [$AgBiTe_2$], two unnamed Au-Bi-Te minerals [$Au_{0.07}Bi_{0.72}Te_{0.21}$] and one unnamed Ag-Bi [$Ag_{0.52}Bi_{0.48}$] mineral (Table A.3). The most common of these are electrum, with 15 grains identified in vein sets M−3, M−4 and M−5. 19 crystals of hessite were identified in vein sets M−3 and M−5. Nine crystals of volynskite were identified in vein set M−3, along with rare empressite and muthmannite, while rare sylvanite and stützite are found in vein sets M−3 and M−5. 87% (by area) of the Au and Ag-bearing minerals identified are enclosed within hydrothermal alteration minerals, most commonly quartz, with 9% present on the boundary between sulphides and hydrothermal silicate minerals and 4% as inclusions within sulphides (Fig. 6d). 93% of the Au and Ag-bearing minerals have rounded spherical or oblate morphologies, with only 7% having angular morphologies. Hessite is commonly in assemblage with electrum +/- PGM. The electrum in the deposit is gold rich, with an average of 85 wt% Au (from SEM-WDS and EPMA-WDS analysis, Tables 7 and A.2), and six crystals of native Au were identified as inclusions within quartz and pyrite crystals, with an average individual crystal area of 11 μm^2.

4.3. Other accessory minerals

Wittichenite [Cu_3BiS_3] is present as inclusions within bornite. Rare crystals of clausthalite [PbSe] were identified on the edges of sulphide crystals in the main stage vein sets. The late stage galena rimming sulphides in the main stage vein sets was shown by EPMA-WDS and SEM-EDS analysis to be a galena-clausthalite solid solution, containing an average of 4.0 wt% Se (Table 7).

Chromite is commonly present in potassic alteration of the early quartz monzonite, with rare Ni-chromite [$(Ni,Co,Fe^{2+})(Cr,Fe^{3+},Al)_2O_4$], and manganochromite [$(Mn,Fe^{2+})(Cr,V)_2O_4$] also identified in potassic alteration using SEM-EDS. Thorite crystals 5–10 μm are present in all samples analysed, and this ties in with the relatively high whole rock XRF Th contents reported for Skouries (Kroll et al. 2002). The thorites are found within potassic alteration, as inclusions in hydrothermal biotite, and associated with disseminated hydrothermal magnetite and orthoclase. This suggests that the thorite is hydrothermal, rather than primary. Rare coffinite [$U(SiO_4)_{1-x}(OH)_{4x}$] is also present in potassic alteration, and Ce and Th rich monazites and zircons were also identified as accessory minerals. The monazites were found in M−3 type veins as inclusions in quartz and in chalcopyrite, suggesting they are hydrothermal in origin.

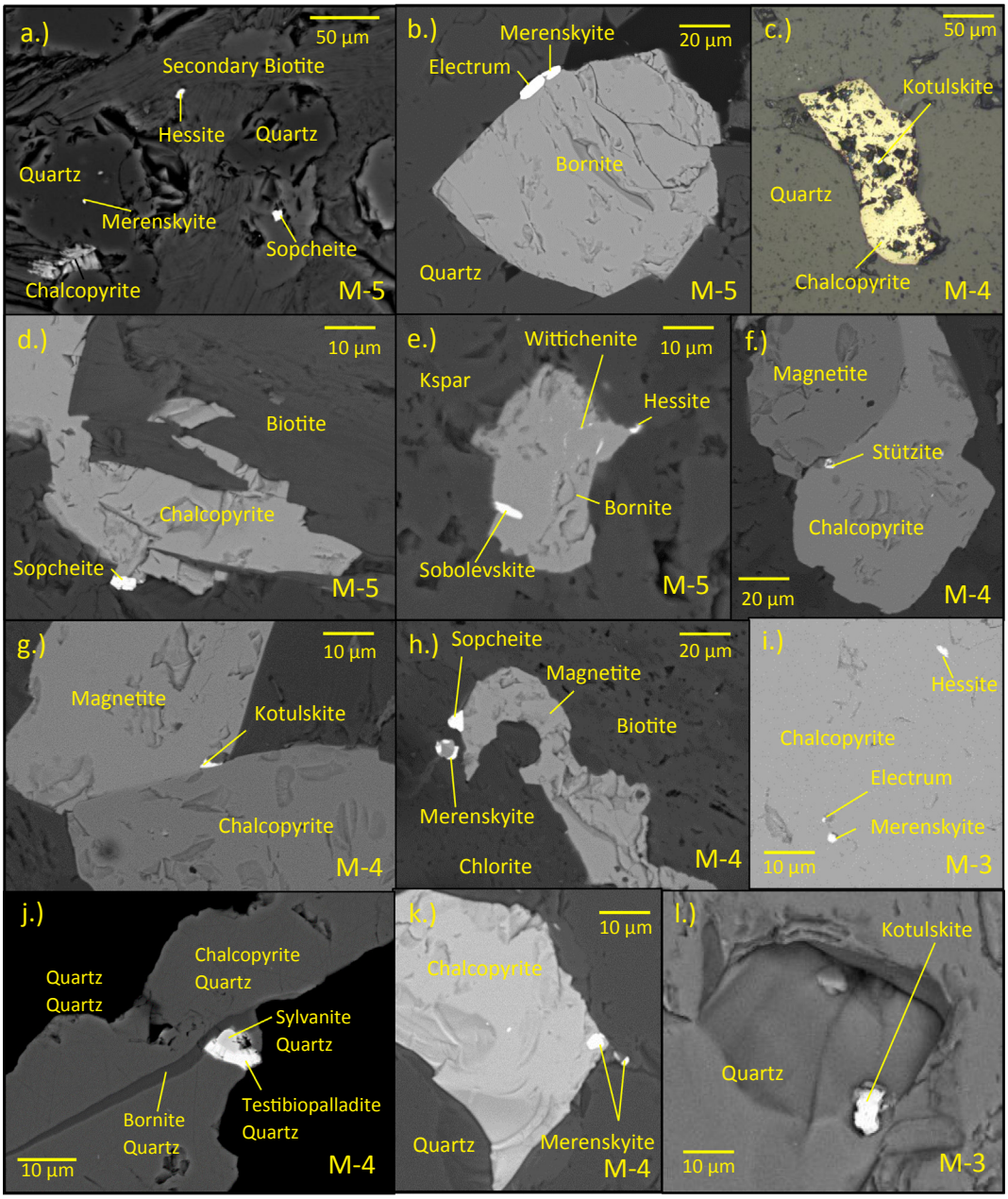

Fig. 5. Backscatter SEM images and reflected microscopy photos of PGM and precious metal-bearing minerals in context with vein type. *Copyright (2016) University of Southampton.*

5. Discussion

The mineralisation and alteration at Skouries is broadly similar to that in other alkali Cu-Au porphyry deposits such as the Ridgeway deposit, New South Wales (Wilson et al., 2003), and the main stage PGM-bearing veins are similar to those in Elatsite, another PGE-enriched Cu-Au porphyry deposit. The observation of PGE-bearing minerals within the main stage of mineralisation agrees with previous work by Tarkian et al. (1991) and by Economou-Eliopoulos and Eliopoulos (2000) but extends the range of recorded minerals. Importantly it provides clear evidence as to PGE deportment and clues as to the underpinning processes responsible.

5.1. PGM in the Skouries deposit

The Skouries porphyry deposit contains a large diversity of PGE-bearing minerals associated with a range of precious metal-bearing minerals and exotic phases, such as chromite, not commonly observed in porphyry Cu deposits. Skouries contains a more varied suite of platinum-group minerals than Elatsite and Santo Tomas II, the two other porphyries to have undergone thorough in-situ platinum-group mineral surveys (Augé et al., 2005; Tarkian and Koopmann, 1995). Skouries is the only porphyry deposit known to contain sobolevskite, telargpalite, isomertieite and testibiopalladite to date. In contrast to other PGE-enriched porphyry deposits where merenskyite is the most common PGM, sopcheite is the most common PGM present in the Skouries deposit. Elatsite contains merenskyite and merenskyite-moncheite solid solutions (Bogdanov et al., 2005; Tarkian et al., 2003), while Santo Tomas II contains merenskyite, kotulskite and moncheite (Tarkian and Koopmann, 1995). Although these deposits also contain a range of silver tellurides, neither of them are reported to contain sopcheite, suggesting the Ag and PGE in those deposits are either transported by different mechanisms or are temporally or spatially separate. There are a wider variety of PGM reported in the porphyry – epithermal transition

Table 5
Results from representative quantitative EPMA-WDS analysis of PGM in wt.%. * = element has undergone empirical correction to eliminate peak overlap. S, Cu and Fe concentrations are interpreted to be background interference from the sulphide host minerals due to the small size of the PGM. *Copyright (2016) University of Southampton.*

Sample	3	3	34	34	36	36	Error (2σ)	Detection limit
PGM #	PGM 1	PGM 2	PGM 1	PGM 2	PGM 1	PGM 2		
S*	19.5	5.3	0.4	1.3	3.0	0.9	0.6	0.07
Pt*	0.59	< dt	< dt	< dt	0.96	2.33	0.24	0.14
Mn	< dt	< dt	< dt	< dt	< dt	< dt	0.05	0.03
Fe	2.8	0.9	0.3	1.3	4.5	1.7	0.2	0.03
Co	< dt	< dt	< dt	< dt	< dt	< dt	0.06	0.03
Ni*	< dt	< dt	< dt	< dt	< dt	< dt	0.06	0.03
Cu*	14.4	2.5	1.1	1.7	3.0	2.2	0.32	0.05
Zn	< dt	< dt	< dt	< dt	< dt	< dt	0.03	0.02
As	< dt	0.40	< dt	< dt	< dt	< dt	0.05	0.03
Se	2.17	2.47	< dt	< dt	< dt	< dt	0.06	0.03
Pd*	20.6	16.0	28.4	32.7	25.2	25.3	0.27	0.08
Ag*	< dt	25.2	< dt	2.36	< dt	0.52	0.31	0.05
Sb*	< dt	2.9	0.1	0.1	0.1	0.1	0.13	0.08
Te*	< dt	22.0	67.1	54.1	61.8	63.1	0.42	0.10
Pb*	< dt	20.9	1.19	< dt	< dt	< dt	0.33	0.14
Bi*	39.7	0.8	< dt	8.7	1.7	3.2	0.50	0.17
Cr	< dt	< dt	< dt	< dt	< dt	< dt	0.06	0.04
Ru	< dt	< dt	< dt	< dt	< dt	< dt	0.18	0.11
Rh*	< dt	0.3	0.8	0.5	0.7	0.8	0.23	0.14
Os*	< dt	< dt	0.3	0.2	0.2	0.2	0.08	0.05
Ir*	< dt	< dt	< dt	< dt	< dt	< dt	0.21	0.12
Au*	0.2	< dt	< dt	< dt	< dt	< dt	0.45	0.19
Si	0.2	0.7	< dt	0.1	< dt	< dt	0.04	0.01
Total	99.3	100.5	98.1	101.6	100.3	99.5		
Mineral	Sobolevskite	Sopcheite	Testibiopalladite	Merenskyite	Merenskyite	Merenskyite		

zone of deposits such as Mount Milligan, with naldrettite and stibiopalladinite present (Lefort et al., 2011), and the Mikheevskoe deposit (South Urals), with merenskyite and rare sopcheite reported (Plotinskaya et al., 2018). Skouries however has the largest variety of PGM reported within the higher temperature potassic alteration zone of a porphyry deposit.

The PGM present in the Skouries deposit are all Pd minerals, with the merenskyites analysed either falling on the Pd end member, or containing approximately 10:1 Pd:Pt. This agrees with previous whole rock PGE studies on Skouries which have reported Pd to Pt ratios of approximately 10:1 (Economou-Eliopoulos and Eliopoulos, 2000; Eliopoulos and Economou-Eliopoulos, 1991), although company assay data provided for this study has an average Pd/Pt of 50, with a range of 20–96. This relative Pd enrichment is present in whole rock data from all other PGE-enriched porphyries (Table 1, Fig. 7; Sotnikov et al., 2001; Tarkian and Stribrny, 1999). These ratios either reflect the relative PGE contents in the source magma (Economou-Eliopoulos and Eliopoulos, 2000), or the fractionation of PGE in the mineralising fluid (Eliopoulos et al., 2014). PGE-enriched porphyry deposits globally have very similar Au/(Pd + Pt) of ~90 and Pd/Pt of ~10 (Fig. 7, Augé et al., 2005, 2002; Eliopoulos et al., 2014; Eliopoulos and Economou-Eliopoulos, 1991; Maier and Bowen, 1996; Steele, 1978; Thompson et al., 2001). However, it is worth noting that the company assay data provided in this study shows no correlation between Au and Pd + Pt (R^2 = 0.01), with an average Au/(Pd + Pt) of 310, meaning that Au grade should not be used as a proxy for PGE grade. PGE-enriched porphyries plot on the same Pd/Pt gradient as barren granitoids which suggests Pd/Pt in these deposits is likely to represent source magma PGE concentrations. However, the Buala Nuasahi deposit, a hydrothermal PGE deposit formed from the remobilisation of PGEs from a layered ultramafic intrusion, also plots on the same Pd/Pt slope (Fig. 7). This suggests that the relative proportions of Pd and Pt may also be a function of their relative hydrothermal mobility. Pd has higher solubility in hydrothermal fluids than Pt (Barnes and Liu, 2012) and experimental work has shown Pt to be almost immobile in chlorine-rich fluids up to 600 °C (Scholten et al., 2018). Both Pd and Pt are more mobile in reducing conditions (as bisulphide complexes) where solubility peaks at neutral pH. However, under oxidised conditions such as those in the fluids which form porphyry deposits both Pd and Pt solubility (as chloride complexes) increases with decreasing pH (Barnes and Liu, 2012). The PGM at Skouries are predominantly Bi-Te minerals, with only 6% containing other semi-metals. This association between PGE and Bi-Te complexes is present in all other PGE-enriched porphyry deposits.

This study has confirmed that the PGE in Skouries are associated with the main vein stage of Cu deposition in this deposit. This agrees with work by Eliopoulos and Economou-Eliopoulos (1991), Eliopoulos et al. (2014), who analysed whole rock samples for PGE content and found the potassic alteration zone to have Pd contents of 60–610 ppb and Pt contents of 5–150 ppb. Earlier work suggested that precious metal tellurides were formed in relatively shallow, cool environments, and that the PGE may have been redistributed during a late hydrothermal event (Eliopoulos and Economou-Eliopoulos, 1991; Mutschler et al., 1985). However, this study shows that no PGE mineralization is present within the late stage veins, or associated with argillic alteration. This is similar to the distribution of platinum-group minerals in other porphyry deposits. PGE in Elatsite, Santo Tomas II, Mamut and Majdanpek deposits are all associated with the main, hypogene mineralisation and with potassic alteration (Tarkian et al., 2003; Tarkian and Koopmann, 1995; Tarkian and Stribrny, 1999). However, there are documented examples of veins bearing PGM in the porphyry-epithermal transition zone. For example, the late stage 'sub-epithermal' veins in the Mount Milligan porphyry deposit, British Columbia contain PGM associated with electrum and Hg-rich pyrite (Lefort et al., 2011), and PGM have also been documented in the epithermal overprint of the Mikheevskoe porphyry deposit (Plotinskaya et al., 2018).

The platinum-group minerals in Skouries are associated with M−3 and M−4 veins, commonly associated with bornite-chalcopyrite-magnetite assemblages, and in M−5 veins associated with bornite-chalcopyrite-pyrite assemblages. The platinum-group minerals in Elatsite and

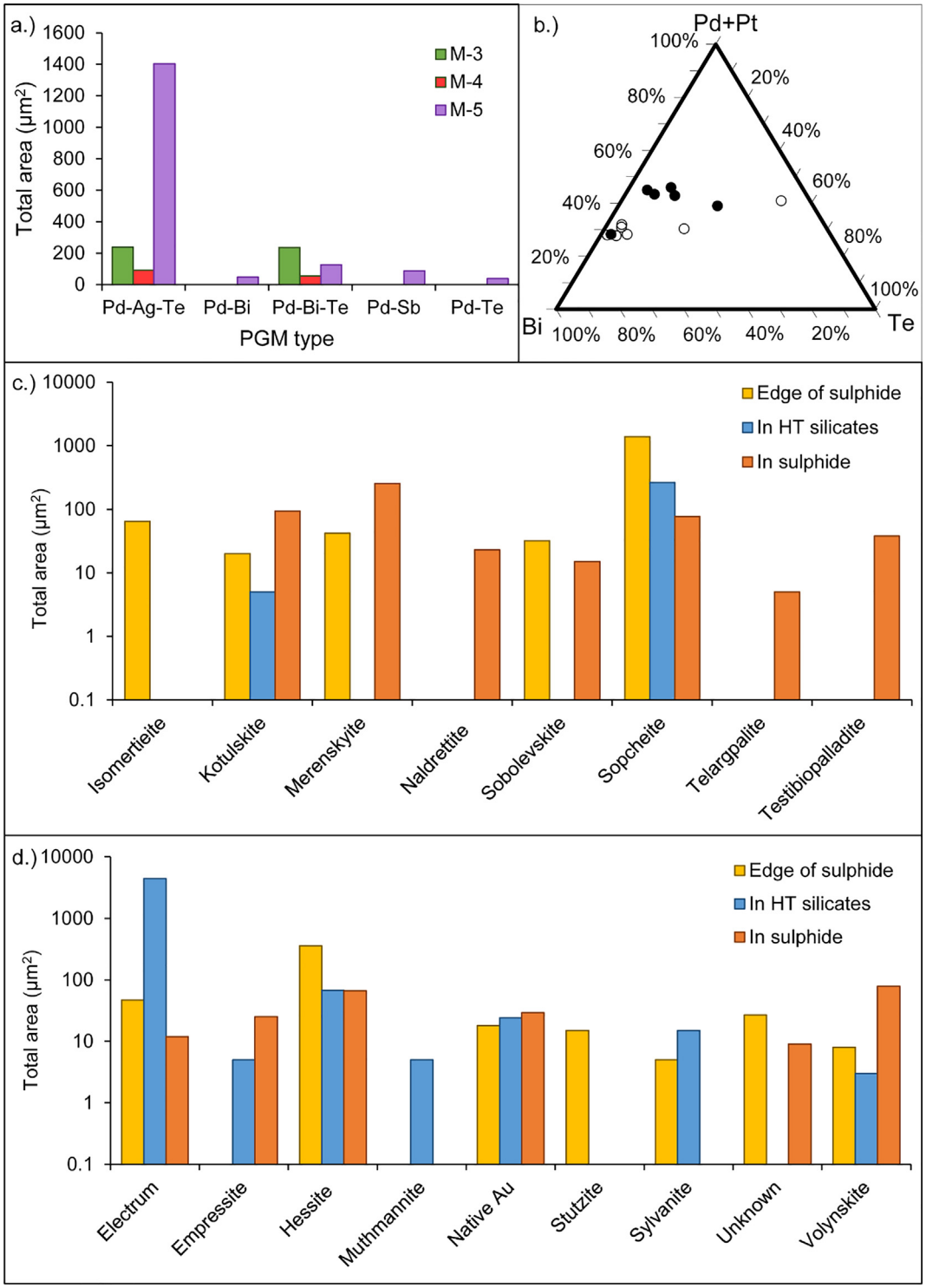

Fig. 6. a.) Graph showing PGM type distribution between vein sets b.) Triplot showing the proportion of semi-metals present in merenskyites [$(Pd,Pt)(Te,Bi)_2$] (solid circles) and kotulskites [Pd(Te,Bi)] (hollow circles) c.) Graph showing the area and association of platinum group minerals in Skouries (HT = hydrothermal) d.) Graph showing the area and association of precious-metal bearing minerals in Skouries. *Copyright (2016) University of Southampton.*

Santo Tomas II (Tarkian et al., 2003; Tarkian and Koopmann, 1995) are also found in chalcopyrite-bornite-magnetite assemblages as inclusions in chalcopyrite. In contrast to these deposits the majority of platinum-group minerals in Skouries are present as discrete crystals on the edge of sulphides and magnetite both within the veins, and in potassic alteration selvages surrounding the M−5 veins. Only 18% of the PGM in Skouries are present as inclusions in sulphides, with a significant number of PGM (15%) enclosed in hydrothermal quartz, biotite and feldspar with no obvious sulphide association. This suggests they were carried by a hydrothermal fluid (Xiong and Wood, 2000), and that their mechanism of transport and/or precipitation was decoupled from that of Cu. The majority of the Skouries PGM have rounded, droplet-like morphologies. These droplets are present as inclusions within the centre of euhedral hydrothermal quartz crystals, and within other minerals

Table 6
Other precious metal-bearing minerals identified in the Skouries deposit (using SEM-EDS and SEM-WDS). HT silicate = hydrothermal alteration silicate mineral. *Copyright (2016) University of Southampton.*

Sample	Vein set	Mineral	Host	Size (μm^2)	Texture	Host type	Type
1	M−3	Muthmannite	Quartz	5	Rounded	In HT silicate	Ag-Au-Te
6	M−3	Hessite	Quartz	4.8	Rounded	In HT silicate	Ag-Te
6	M−3	Hessite	Quartz	3.1	Rounded	In HT silicate	Ag-Te
6	M−3	Hessite	Quartz	4	Rounded	In HT silicate	Ag-Te
6	M−3	Hessite	Pyrite	15	Angular	Edge of sulphide	Ag-Te
6	M−3	Hessite	Pyrite	7	Angular	Edge of sulphide	Ag-Te
6	M−3	Unknown	Chalcopyrite	27	Rounded	Edge of sulphide	Ag-Bi
8	M−3	Electrum	Quartz	10	Rounded	In HT silicate	Au-Ag
8	M−3	Empressite	Biotite	5	Rounded	In HT silicate	Ag-Te
8	M−3	Hessite	Pb-Se-S	15	Rounded	In sulphide	Ag-Te
8	M−3	Sylvanite	Quartz	10	Rounded	In HT silicate	Ag-Au-Te
9	M−3	Native Au	Pyrite	29	Rounded	In sulphide	Au
11	M−5	Electrum	Quartz	30	Rounded	In HT silicate	Au-Ag
11	M−5	Electrum	Quartz	2.2	Rounded	In HT silicate	Au-Ag
11	M−5	Electrum	Quartz	1.6	Rounded	Edge of sulphide	Au-Ag
11	M−5	Electrum	Quartz	7	Rounded	In HT silicate	Au-Ag
11	M−5	Hessite	Quartz	150	Angular	Edge of sulphide	Ag-Te
11	M−5	Hessite	Quartz	8.5	Rounded	Edge of sulphide	Ag-Te
11	M−5	Hessite	Quartz	150	Angular	Edge of sulphide	Ag-Te
11	M−5	Hessite	Chalcopyrite	18	Angular	In sulphide	Ag-Te
11	M−5	Native Au	Quartz	5.4	Rounded	In HT silicate	Au
11	M−5	Native Au	Quartz	5.8	Rounded	In HT silicate	Au
11	M−5	Native Au	Kspar	5	Rounded	In HT silicate	Au
11	M−5	Native Au	Quartz	18	Rounded	Edge of sulphide	Au
11	M−5	Native Au	Quartz	8	Angular	In HT silicate	Au
13	M−3	Unknown	Pyrite	5	Rounded	In sulphide	Au-Te-Bi
13	M−3	Unknown	Pyrite	3.5	Rounded	In sulphide	Au-Te-Bi
31	M−4	Electrum	Quartz	10	Rounded	Edge of sulphide	Au-Ag
34	M−5	Electrum	Chalcopyrite	10	Rounded	In sulphide	Au-Ag
34	M−5	Electrum	Quartz	10	Rounded	Edge of sulphide	Au-Ag
34	M−5	Electrum	Quartz	10	Rounded	Edge of sulphide	Au-Ag
34	M−5	Electrum	Quartz	10	Rounded	In HT silicate	Au-Ag
34	M−5	Electrum	Chalcopyrite	1.7	Rounded	In sulphide	Au-Ag
34	M−5	Electrum	Clay	1.5	Rounded	In HT silicate	Au-Ag
34	M−5	Electrum	Quartz	15	Rounded	Edge of sulphide	Au-Ag
34	M−5	Electrum	Quartz	2	Rounded	In HT silicate	Au-Ag
34	M−5	Hessite	Chalcopyrite	4	Rounded	In sulphide	Ag-Te
34	M−5	Hessite	Pb-Se-S	5.7	Rounded	In sulphide	Ag-Te
34	M−5	Stützite	Magnetite	15	Rounded	Edge of sulphide	Ag-Te
34	M−5	Sylvanite	Quartz	5	Rounded	Edge of sulphide	Ag-Au-Te
34	M−5	Sylvanite	Quartz	5	Rounded	In HT silicate	Ag-Au-Te
36	M−3	Electrum	Quartz	4360	Rounded	In HT silicate	Au-Ag
36	M−3	Empressite	Chalcopyrite	25	Rounded	In sulphide	Ag-Te
36	M−3	Hessite	Chalcopyrite	10	Rounded	In sulphide	Ag-Te
36	M−3	Hessite	Chalcopyrite	15	Rounded	Edge of sulphide	Ag-Te
36	M−3	Hessite	Chalcopyrite	11	Rounded	Edge of sulphide	Ag-Te
36	M−3	Hessite	Chalcopyrite	13	Rounded	In sulphide	Ag-Te
36	M−3	Hessite	Quartz	8	Rounded	In HT silicate	Ag-Te
36	M−3	Hessite	Quartz	34	Rounded	In HT silicate	Ag-Te
36	M−3	Hessite	Quartz	14	Rounded	In HT silicate	Ag-Te
36	M−3	Volynskite	Chalcopyrite	1.7	Rounded	In sulphide	Ag-Te-Bi
36	M−3	Volynskite	Chalcopyrite	8	Rounded	Edge of sulphide	Ag-Te-Bi
36	M−3	Volynskite	Chalcopyrite	14	Rounded	In sulphide	Ag-Te-Bi
36	M−3	Volynskite	Chalcopyrite	46	Rounded	In sulphide	Ag-Te-Bi
36	M−3	Volynskite	Chalcopyrite	4.5	Rounded	In sulphide	Ag-Te-Bi
36	M−3	Volynskite	Chalcopyrite	1.6	Angular	In sulphide	Ag-Te-Bi
36	M−3	Volynskite	Chalcopyrite	3	Rounded	In sulphide	Ag-Te-Bi
36	M−3	Volynskite	Chalcopyrite	7.6	Rounded	In sulphide	Ag-Te-Bi
36	M−3	Volynskite	Quartz	3	Angular	In HT silicate	Ag-Te-Bi

precipitated from the hydrothermal fluid (Fig. 5), suggesting that they were trapped as molten droplets and solidified as the liquid cooled (Ciobanu et al., 2005).

5.2. The role of semi-metals in PGE enrichment

One of the problems associated with the formation of PGE-enriched porphyries is that it is very unlikely that hydrothermal fluids will contain enough Pd to reach saturation in order to allow PGM to precipitate directly and be incorporated into quartz rather than within sulphides (Bazarkina et al., 2014). This means an additional mechanism is needed that both sequesters the PGE more strongly than sulphide and allows the metals to remain associated with the hydrothermal fluid in high enough concentrations to precipitate the PGM directly from the fluid when conditions permit.

In principle, co-existing polymetallic melts in hydrothermal systems can partition metals from the fluid and concentrate them as melt components (Douglas, 2000), and sulfosalt melts have been shown to

Table 7
Results from quantitative EPMA-WDS analysis of precious metal minerals in wt.%. *= element has undergone empirical correction to eliminate peak overlap. Cu and Fe concentrations are interpreted to be background interference from the sulphide host minerals due to the small size of the minerals. PMM = precious metal mineral; GAL = galena. *Copyright (2016) University of Southampton.*

Sample	34	34	34	34	36	34	Error (2σ)	Detection limit
MIN #	PMM 1	PMM 2	PMM 3	PMM 4	PMM 2	GAL 1		
S*	< dt	< dt	< dt	0.5	0.9	14.8	0.6	0.07
Pt*	< dt	< dt	< dt	< dt	< dt	< dt	0.24	0.14
Mn	< dt	< dt	< dt	< dt	< dt	< dt	0.05	0.03
Fe	0.7	0.5	0.3	0.2	2.4	7.1	0.2	0.03
Co	< dt	< dt	< dt	0.23	< dt	< dt	0.06	0.03
Ni*	< dt	< dt	< dt	0.21	< dt	0.2	0.06	0.03
Cu*	0.9	0.5	0.3	2.8	2.5	7.5	0.32	0.05
Zn	< dt	< dt	< dt	< dt	< dt	< dt	0.03	0.02
As	< dt	< dt	< dt	< dt	< dt	< dt	0.05	0.03
Se	< dt	< dt	< dt	0.86	0.11	4.0	0.06	0.03
Pd*	< dt	< dt	< dt	< dt	< dt	< dt	0.27	0.08
Ag*	19.2	17.2	16.1	54.8	58.7	< dt	0.31	0.05
Sb*	< dt	< dt	< dt	0.1	< dt	< dt	0.13	0.08
Te*	0.63	< dt	< dt	37.2	37.5	< dt	0.42	0.10
Pb*	< dt	< dt	< dt	3.0	< dt	61.1	0.33	0.14
Bi*	< dt	< dt	< dt	< dt	0.6	0.9	0.50	0.17
Cr	< dt	< dt	< dt	< dt	< dt	< dt	0.06	0.04
Ru	< dt	< dt	< dt	< dt	< dt	< dt	0.18	0.11
Rh*	< dt	< dt	< dt	0.5	0.4	< dt	0.23	0.14
Os*	< dt	< dt	< dt	0.1	0.1	0.5	0.08	0.05
Ir*	< dt	< dt	< dt	< dt	< dt	0.2	0.21	0.12
Au*	80.9	84.1	85.4	< dt	< dt	< dt	0.45	0.19
Si	0.06	< dt	0.1	< dt	< dt	0.2	0.04	0.01
Total	101.8	102.3	102.2	98.8	102.5	96.5		
Mineral	Electrum	Electrum	Electrum	Stützite	Hessite	Galena		

have condensed from expanding magmatic vapour at temperatures of ~650 °C in the El Indio paleo-fumarole (Henley et al., 2012; Henley and Berger, 2013; Mavrogenes et al., 2010). Semi-metals like Bi and Te at high concentrations can act as powerful fluxes, lowering the melting point of metals such as Au and the PGE - for example the Au-Bi melt has a eutectic at 241 °C (Gather and Blachnik, 1974; Okamoto and Massalski, 1983). This has led to bismuth being suggested as a 'collector' for Au in hydrothermal fluids (e.g. Douglas 2000; Cockerton and Tomkins 2012; Tooth et al. 2008), acting as an independent enrichment mechanism and allowing the formation of hydrothermal ore deposits from fluids that would otherwise be under-saturated in Au. Experimental studies have shown that in Au-Bi-Na-Cl-S-H-O systems, Au preferentially partitions into an Au-Bi melt rather than the fluid (Tooth et al., 2011, 2008), and natural examples of liquid bismuth co-existing with hydrothermal fluid have been reported (Cockerton and Tomkins, 2012). Au-Bi melts are only present in a limited range of fO_2 conditions, however it is thought that Bi-Te melts may act as Au scavengers in high fO_2 conditions, as native tellurium stability is coincident with hematite (Ciobanu et al., 2005; Grundler et al., 2013). Thermodynamic modelling work has shown that at high temperatures (550 °C) an Au-Bi-Te melt will precipitate from an Au-Bi-Te-S-C-Cl-Na-K-Ca-O–H fluid, even when the fluid is moderately under-saturated with Au, Bi and Te (Wagner, 2007). Bi-Te melts have eutectics of 266 °C (Bi-rich), and 413 °C (Te-rich) (Ciobanu et al., 2005), both within the range of temperatures analysed in porphyry hydrothermal fluids (Wilkinson, 2001). Bi-Te-(+/-Au) droplets have been identified in hydrothermal quartz crystals in deposits such as the Batman Au deposit, Australia; the Bi-Au Stormont skarn deposit, Tasmania and the Larga hydrothermal system, Romania (Cockerton and Tomkins, 2012; Cook and Ciobanu, 2004; Hein et al., 2006) implying they were precipitated in a molten state (Ciobanu et al., 2005; Mavrogenes et al., 2010).

Palladium partitions strongly into semi-metal melts in the magmatic environment even in the presence of a strong sulphide collector mineral such as pentlandite (Helmy et al., 2007; Holwell and McDonald, 2010). Porphyry systems lack significant pentlandite, removing a potential sulphide host for Pd and increasing the tendency for it to combine with semi-metals in porphyry deposits, rather than be hosted in the sulphides (Eliopoulos et al., 2014; Tarkian et al., 2003; Tarkian and Koopmann, 1995; Tarkian and Stribrny, 1999; Thompson et al., 2001). The Pd-Bi-Te system is molten above 489 °C (Cabri, 1981; Cabri and Harris, 1973), which is within the temperature range of porphyry system hydrothermal fluids generally (e.g. Wilkinson, 2001), and within the range of fluid inclusion temperatures for the Skouries deposit (350 °C – > 600 °C; Frei, 1995; McFall et al., 2017). It appears likely that this semi-metal collector mechanism could also scavenge PGE from fluids, concentrating them into a co-existing semi-metal melt.

In order to account for the textural observations at Skouries and other porphyry deposits a model is proposed whereby Pd is scavenged from high temperature (> 490 °C) hydrothermal fluids by a co-existing Bi-Te melt. This creates a Pd-Bi-Te melt which crystallises as palladium bismuthides, tellurides and tellurobismuthides according to the phase diagrams in Cabri (1981). Almost all of the PGM in the Skouries, Elatsite and Santo Tomas II deposits, and indeed in other PGE-enriched porphyries globally, are PGE-Bi-Te minerals, rather than PGE-rich sulphides or minerals containing other semi-metals such as As. The PGM in Skouries are present as rounded inclusions within the centre of euhedral hydrothermal quartz crystals, and within other minerals precipitated from the hydrothermal fluid, and are therefore proposed to represent solidified melt droplets. This model requires both Bi and Te to be present as the Pd-Te binary system is only molten above 720–740 °C (Cabri, 1981; Hoffman and Maclean, 1976), and the Pd-Bi binary system is only molten above 620 °C (Cabri, 1981). Binary systems of palladium with other semi-metals also only produce melts above the temperatures present in porphyry fluids – the Pd-Sb binary system is only molten above 800 °C, the Pd-As system is only molten above 835 °C and the Pd-Se system is only molten above 678 °C (Cabri, 1981), although depending on phase ratios some binary phases may occur at lower temperatures.

The most abundant PGM in Skouries is sopcheite, showing Ag to be a major component of any melt phase. The ternary system Pd-Ag-Te has

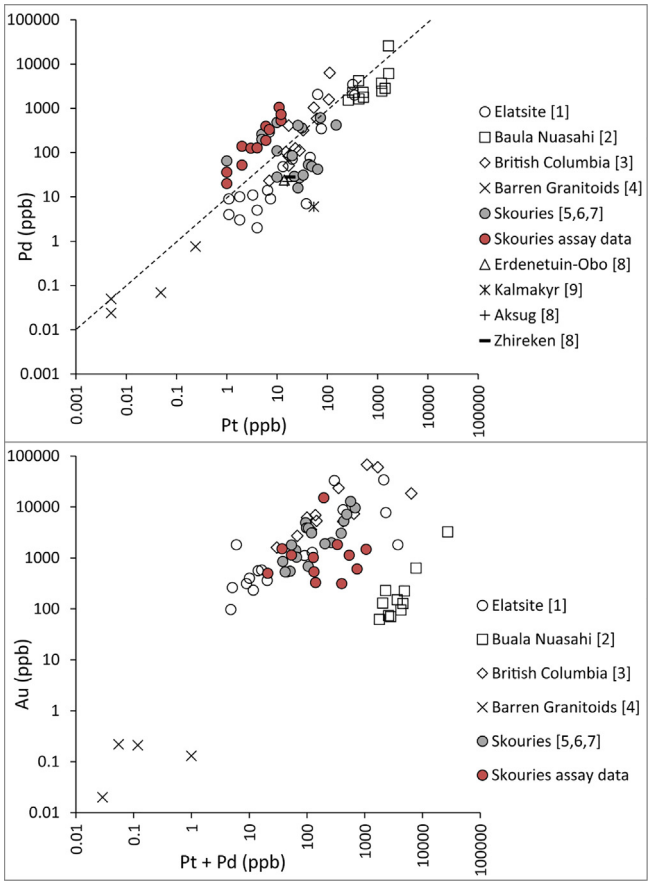

Fig. 7. Comparison of whole rock Au, Pt and Pd analyses from Skouries (grey symbols from earlier studies, red symbols from Eldorado Gold Corp. assay data) with other ore deposits results: PGE-enriched porphyries Elatsite, Santo Tomas II and the British Columbia region porphyries, barren granitoids, and a hydrothermally-modified layered ultra-mafic intrusion Buala Nuasahi. The dotted line represents Pd:Pt of 10:1 (Data from Augé et al., 2005[2], 2002[1]; Economou-Eliopoulos and Eliopoulos, 2000[5]; Eliopoulos et al., 2014[6]; Eliopoulos and Economou-Eliopoulos, 1991[7]; Pašava et al., 2010[9]; Sotnikov et al., 2001[8]; Steele, 1978[4]; Thompson et al., 2001[3]). *Skouries assay data reproduced with permission of Eldorado Gold Corporation, Vancouver, Canada. Copyright (2016) University of Southampton.*

been modelled, with sopcheite shown to be stable up to 383 °C, and to form assemblages with kotulskite and hessite (as in Skouries) at 350 °C (Vymazalová et al., 2015). This provides an upper limit for the temperature of formation of the PGM assemblages containing sopcheite, meaning that these must have formed as the co-melt cooled to below 383 °C. Phase diagrams have yet to be defined for the full range of ternary and quaternary PGE–semi-metal systems and so it is possible that there may also be other complexes which have a low enough melting point to act as a PGE collector.

It is also worth noting that the mineralising fluids in porphyry Cu deposits are commonly high-salinity (> 30 wt%), and high temperature (> 350 °C) with a relatively high oxygen fugacity. These are conditions which favour the hydrothermal transport of Pd as a Cl complex (Xiong and Wood, 2000). Although it has been shown that Au-Bi-Te melts will precipitate from high temperature and salinity hydrothermal fluids undersaturated in Au (Wagner, 2007). To date no modelling or experimental work has been done on the complex Pd-Bi-Te-S-C-Cl-Na-K-Ca-O–H system. It is therefore unclear what effect the co-existing fluid would have on a Pd-Bi-Te melt and what temperature, salinity and oxygen fugacity conditions would allow the precipitation of a Pd-Bi-Te co-melt.

Nonetheless the ubiquitous association of Pd with Bi-Te assemblages in porphyry deposits may provide an exploration indicator for PGE-enriched porphyry deposits, as high Bi and Te contents in assay may indicate the presence of microscopic platinum-group minerals which may be overlooked during standard ore characterisation if the PGE are not assayed. Although PGE in porphyries globally have been reported to be hosted in semi-metal platinum-group minerals (Tarkian and Stribrny, 1999), there is a paucity of data on the Te and Bi content of PGE-enriched porphyry systems, or indeed the semi-metal content of porphyry systems generally. Skouries is rich in semi-metals, with Bi concentrations in ore samples of between 0.1 and 390 ppm and Te concentrations of 0 to 16 ppm. Elatsite has Bi concentrations in ore samples of between 0.2 and 291 ppm, and Te concentrations between 0.2 ppm and 3.8 ppm, with a positive correlation reported between Pd, Au, Te and Bi (Tarkian et al., 2003) suggesting that similar semi-metal collector mechanisms may have been operating. However, more data is needed on semi-metal and PGE concentrations in porphyry deposits globally in order to test this hypothesis.

5.3. Other precious metals

The presence of inclusions of droplet-shaped Bi-Te minerals within hydrothermal quartz and sulphides in the Skouries deposit supports the hypothesis that a Bi-Te immiscible melt was present. If this was the case then it would be expected to scavenge Au, and potentially Ag, as well as Pd from the fluid. A range of Au and Ag tellurides and bismuth-tellurides are present in the Skouries deposit, including volynskite ($AgBiTe_2$) and an unnamed Au-Bi-Te mineral [$Au_{0.07}Bi_{0.72}Te_{0.21}$]. These Au-Bi-Te minerals have compositions which are more Bi-rich than the melt compositions calculated for Au-Bi-Te precipitating from a 550 °C multi-cation hydrothermal fluid [$Au_{0.04}Bi_{0.46}Te_{0.50}$]. They have similar Au levels, and melts with higher Bi concentrations have been shown to precipitate from fluids with a higher starting Bi concentration (Wagner, 2007). Almost all of the precious metal-bearing minerals in the Skouries deposit have droplet-like spherical morphologies and are present as inclusions in the centre of hydrothermal quartz crystals and other hydrothermal alteration minerals, such as secondary biotite. The most abundant precious metal minerals in the Skouries deposit are hessite and electrum, which are often found together. The Au-Ag-Te ternary system has been shown to be molten at temperatures > 435 °C (Cabri, 1965), which is within the range of temperatures for main stage ore-forming veins in porphyries. If these minerals were formed from the cooling of a melt then this puts temperature constraints on the system as hessite and electrum co-exist at temperatures > 550 °C (Markham, 1960). Sylvanite, however, is only stable up to 360 °C (Markham, 1960) while empressite is stable up to 191 °C (+/-16°) (Voronin et al., 2017). The presence of these relatively low temperature minerals is interpreted to represent the changing composition of the co-melt as the system cooled. The range of tellurides present in Skouries suggest the initial co-melt contained Au-Ag-Pd-Te-Bi. This is proposed to have precipitated native Au, electrum-hessite assemblages and Au-Bi-Te minerals as the system cooled below ~540 °C, removing the majority of the Au from the melt (Markham, 1960; Voronin et al., 2017; Wagner, 2007). This would leave a Pd-Ag-Te-Bi-(Au) melt which could precipitate merenskyite-hessite and kotulskite-hessite assemblages as the system cooled below 450 °C, followed by sopcheite-kotulskite-hessite assemblages below 383 °C (Vymazalová et al., 2015). This would remove most of the Pd and Bi, leaving a Ag-Te-(Pd-Bi-Au) melt which could precipitate sylvanite and rare merenskyite-stützite assemblages as it cooled past 350 °C (Markham, 1960; Vymazalová et al., 2015), leaving an Ag-Te melt phase which could form empressite below 200 °C (Voronin et al., 2017).

The varied suite of precious metal and semi-metal bearing accessory minerals present in Skouries has also been observed in Elatsite and Santo Tomas II, giving further evidence that PGE-enriched porphyry deposits contain an abundance of semi-metals. Stützite, empressite,

hessite and sylvanite are all also present in Elatsite, with only muthmannite and volynskite unique to the Skouries deposit (Augé et al., 2005; Bogdanov et al., 2005; Tarkian et al., 2003; Tarkian and Koopmann, 1995). Skouries also contains wittichenite and clausthalite, both of which are observed at Elatsite (Bogdanov et al., 2005). Elatsite however also contains native Te and bohdanowiczite ($AgBiSe_2$), neither of which are observed at Skouries, while Santo Tomas II contains relatively abundant selenides (Tarkian and Koopmann, 1995). This suggests that Skouries is a more Bi-rich and Se-poor system than Elatsite and Santo Tomas II.

6. Conclusions

The Skouries Cu-Au deposit is a multi-stage alkali porphyry system with multiple overprinting intrusions, each associated with hydrothermal vein sets. These can be divided into 'early stage' vein sets, which comprise predominantly quartz–magnetite ± pyrite–chalcopyrite veins associated with intense potassic alteration of a host monzonite intrusion. The main Cu and Au mineralisation is associated with the 'main stage' vein sets which are associated with syn-mineralisation syenite intrusions. Three vein sets host the majority of the mineralisation – M − 3, quartz–massive chalcopyrite ± bornite veins; M − 4, quartz–magnetite–chalcopyrite–bornite veins and M − 5, quartz–chalcopyrite–bornite veins with the sulphides in a central suture. These are all associated with potassic alteration and are followed by 'late stage' vein sets which are associated with phyllic alteration assemblages.

The Skouries deposit is unusually PGE-enriched, with a very high Pd to Pt ratio. This is due to the presence of Pd minerals in the main mineralising vein sets, M − 3, M − 4 and M − 5, associated with potassic alteration minerals. The platinum-group minerals in Skouries have been identified as sopcheite [$Ag_4Pd_3Te_4$], merenskyite [(Pd,Pt)(Te,$Bi)_2$] and kotulskite [Pd(Te,Bi)], with rare telargpalite [$(Pd,Ag)_3Te$], isomertieite [$Pd_{11}Sb_2As_2$], naldrettite [Pd_2Sb], testibiopalladite [PdTe(Sb,Te)], and sobolevskite [PdBi]. The most common platinum-group mineral is sopcheite and the Skouries deposit contains a greater variety of PGM than reported for other PGE-enriched porphyries. The platinum-group minerals in Skouries are small, 52 μm^2 on average. They are hosted predominantly as spherical minerals on the boundary between sulphides and silicates, but also as inclusions within hydrothermal quartz crystals and sulphides. This evidence shows the Pd and Pt in this deposit is part of the same mineralising event as the Cu and Au, and confirms findings that PGE mineralisation in porphyries is a hypogene event associated with potassic alteration.

Skouries contains a variety of other precious-metal and semi-metal minerals, with electrum [$Au_{0.85}Ag_{0.15}$], empressite [AgTe], hessite [Ag_2Te], stützite [Ag_5-xTe_3, (x = 0.24–0.36)], muthmannite [$AgAuTe_2$], sylvanite [$(Au,Ag)_2Te_4$] and volynskite [$AgBiTe_2$] having been identified as accessory minerals. These precious-metal and semi-metal minerals are found in all the main stage mineralising vein sets, primarily as spherical inclusions in hydrothermal quartz crystals and in ore minerals, and are often associated with platinum-group minerals.

A semi-metal collector model is proposed for PGE in porphyry deposits, whereby an immiscible Bi-Te melt exsolves and acts as a collector for PGE and other precious metals in high temperature (> 490 °C) hydrothermal fluids and precipitates Pd tellurides and bismuthides upon cooling. This would allow the formation of PGE-enriched porphyries without Pt and Pd fluid saturation, and is supported by the occurrence of droplet-shaped Pd-Bi-Te minerals in the centre of euhedral hydrothermal quartz crystals. High concentrations of Bi and Te could be used to indicate the potential presence of PGE in porphyry Cu deposits.

7. Acknowledgements

We would like to acknowledge the Dr Richard Pearce and Dr Duncan Muir for their support on the SEM at the University of Southampton and Cardiff University respectively, Mr John Ford and Mr Robert Jones for thin section preparation. Many thanks are also due to Eldorado Gold Corporation and the team at the Skouries site for logistical support in the field. Dr Robert Knight, Dr Robert Moritz and Dr Tom Gernon are also gratefully acknowledged for their helpful discussions on this manuscript. Dr Panagiotis Voudouris, Dr John Bowles, Dr Cristiana Ciobanu and one anonymous reviewer are gratefully acknowledged for their helpful and constructive reviews. This work was funded by the University of Southampton Mayflower Scholarship, with a contribution from the BGS University Funding Initiative (S219) and by a NERC SoS Consortium grant NE/M010848/1 "TeaSe: tellurium and selenium cycling and supply" awarded to Cardiff University. JN publishes with the permission of the Executive Director, British Geological Survey (NERC).

A.

See Tables A.1–A.3.

Table A.1
Accuracy and precision for the EPMA data. Analysis performed at the Natural History Museum, London (NHM) with values calculated from NHM in-house pure element standards. STD = published standard values; $\bar{x}$ = mean value measured; σ_x = standard deviation in standard measurements; %RSD = standard deviation as a percentage of the published value (precision); %RD = difference of measurement with published value as a percentage of published value (accuracy). *Copyright (2016) University of Southampton.*

Element	STD (wt.%)	$\bar{x}$ (wt.%)	σ_x	%RSD	%RD
Pt	100	99.41	0.11	0.11	0.59
Pd	100	99.76	0	0	0.24
Au	100	99.58	0.19	0.19	0.42
Ag	100	99.77	0.2	0.2	0.23
Bi	53	52.82	0.11	0.09	0.35
Te	47	47.75	0.04	0.24	1.6
Se	27	27.72	0.02	0.02	0.35
Pb	73	72.75	0.02	0.05	2.65
Cu	100	100.86	0.01	0	0.85

Table A.2
Analytical SEM-EDS data (in wt.%) for platinum group minerals with mineral identification. *Copyright (2016) University of Southampton.*

Sample	PGM #	Mineral	Pd	Pt	Ag	Bi	Te	Sb	As	Au	Se
3	PGM1	Sobolevskite	36			64					
3	PGM2	Sobolevskite	38			62					
3	PGM4	Sobolevskite	34	1		65					
3	PGM5	Sopcheite	25		39	2	34				
3	PGM6	Sopcheite	17		66		17				
6	PGM1	Kotulskite	45			6	49				
6	PGM2	Merenskyite	27	1		2	70				
6	PGM3	Sopcheite	28		11	11	51				
8	PGM1	Kotulskite	45			6	49				
9	PGM1	Kotulskite	19		27	13	41				
9	PGM2	Sopcheite	9		14	7	17			53	
9	PGM3	Kotulskite	28			3	68				
9	PGM4	Sopcheite	22		12	8	57				
11	PGM1	Sopcheite	6		57	8	29				
11	PGM2	Sopcheite	9		45	21	24				
11	PGM3	Isomertieite?	70		4			15	11		
11	PGM4	Naldrettite?	63		6		2	15	1		
11	PGM5	Sopcheite	34		5	61	1				
11	PGM6	Kotulskite	43			9	47				
26	PGM1	Sopcheite	17		16	47	21				
31	PGM1	Sopcheite	26		2	29	43				
31	PGM2	Sopcheite	22		17	11	31			20	
31	PGM3	Sopcheite	18		15	11	36			21	
31	PGM4	Merenskyite	29	2		25	45				
31	PGM5	Telargpalite	32		3		66				
31	PGM6	Kotulskite	39			31	30				
34	PGM1	Testibiopalladite	28			67					
34	PGM10	Sopcheite	23		21	8	18				
34	PGM11	Sopcheite	9		40	22	29				
34	PGM12	Sopcheite	26		6	8	60				
34	PGM13	Kotulskite	30			11	29				
34	PGM14	Kotulskite	29				71				
34	PGM15	Kotulskite	43			9	47				
34	PGM16	Sopcheite	19		12	45	24				
34	PGM2	Merenskyite	13			2	25				
34	PGM3	Merenskyite	41			50	9				
34	PGM6	Sopcheite	26		12	6	55				
34	PGM9	Merenskyite	31			5	64				
36	PGM1	Merenskyite	26	2		5	68				
36	PGM12	Sopcheite	11		2	54	29				4
36	PGM18	Merenskyite	25	3		8	63				
36	PGM2	Merenskyite	25	3		8	63				
36	PGM3	Merenskyite	25	3		8	63				
36	PGM4	Merenskyite	25	3		8	63				
36	PGM5	Sopcheite	28		11	11	51				

Table A.3
Analytical SEM-EDS data (in wt.%) for precious metal minerals with mineral identification. *Copyright (2016) University of Southampton.*

Sample	Mineral	Au	Ag	Te	Bi
1	Muthmannite	5	63	31	
6	Hessite		62	38	
6	Hessite		62	38	
6	Hessite		62	38	
6	Hessite		60	40	
6	Hessite		60	40	
6	Unknown		51	1	48
8	Electrum	74	26		
8	Empressite		46	54	
8	Hessite		66	44	
8	Sylvanite	71	25	4	
9	Native Au	100			
11	Native Au	93	7		
11	Electrum	83	27		
11	Electrum				
11	Electrum	78	22		
11	Hessite		74	26	
11	Hessite		66	44	
11	Hessite				
11	Hessite		63	37	
11	Native Au	100			
11	Native Au	100			
11	Native Au	100			
11	Native Au	100			
11	Native Au	100			
13	Unknown	7		21	72
13	Unknown	7		21	72
31	Electrum	70	30		
34	Electrum	74	26		
34	Native Au	84	16		
34	Native Au	84	16		
34	Native Au	86	14		
34	Electrum	77	23		
34	Native Au	86	14		
34	Native Au	99	1		
34	Native Au	99	1		
34	Hessite		95	5	
34	Hessite		70	30	
34	Stützite		57	43	
34	Sylvanite	63	26	11	
34	Sylvanite	49	15	36	
36	Electrum	97	3		
36	Empressite		46	54	
36	Hessite		63	37	
36	Hessite		55	45	
36	Hessite		61	39	
36	Hessite		56	44	
36	Hessite		27	73	
36	Hessite		61	37	1
36	Hessite		62	38	
36	Volynskite		46	42	12
36	Volynskite		29	6	65
36	Volynskite		22	15	63
36	Volynskite		64	36	
36	Volynskite		22	29	49
36	Volynskite		20	27	53
36	Volynskite		32	30	37
36	Volynskite		47	37	15
36	Volynskite		19	9	72

References

Augé, T., Bailly, L., Cocherie, A., Genna, A., Guerrot, C., Lerouge, C., Mukherjee, M.M., Patra, R.N., 2002. Magmatic and hydrothermal Platinum-group element mineralization in the Baula area, Orissa, India. In: Proceedings of the 9th International Platinum Symposium, Billings, Montana, USA, pp. 21–24.

Augé, T., Petrunov, R., Bailly, L., 2005. On the origin of the PGE mineralization in the elatsite porphyry Cu-Au deposit, Bulgaria: Comparison with the baula-nuasahi complex, India, and other alkaline PGE-rich porphyries. Can. Mineral. 43, 1355–1372. http://dx.doi.org/10.2113/gscanmin.43.4.1355.

Barnes, S.J., Liu, W., 2012. Pt and Pd mobility in hydrothermal fluids: evidence from komatiites and from thermodynamic modelling. Ore Geol. Rev. 44, 49–58. http://dx.doi.org/10.1016/j.oregeorev.2011.08.004.

Bath, A.B., Cooke, D.R., Friedman, R.M., Faure, K., Kamenetsky, V.S., Tosdal, R.M., Berry, R.F., 2014. Mineralization, U-Pb Geochronology, and Stable Isotope Geochemistry of the Lower Main Zone of the Lorraine Deposit, North-Central British Columbia: A Replacement-Style Alkalic Cu-Au Porphyry. Econ. Geol. 109, 979–1004.

Bazarkina, E.F., Pokrovski, G.S., Hazemann, J.-L., 2014. Structure, stability and geochemical role of palladium chloride complexes in hydrothermal fluids. Geochim. Cosmochim. Acta 146, 107–131.

Berzina, A.N., Sotnikov, V.I., Economou-Eliopoulos, M., Eliopoulos, D.G., 2007. First finding of merenskyite (Pd, Pt) Te2 in porphyry Cu-Mo ores in Russia. Russ. Geol. Geophys. 48, 656–658.

Bogdanov, K., Filipov, A., Kehayov, R., 2005. Au-Ag-Te-Se minerals in the Elatsite porphyry-copper deposit, Bulgaria. Geochem. Mineral. Petrol. 14–19.

Brun, J.P., Sokoutis, D., 2007. Kinematics of the Southern Rhodope Core Complex (North Greece). Int. J. Earth Sci. 96, 1079–1099. http://dx.doi.org/10.1007/s00531-007-

0174-2.
Burg, J-P. 2012. Rhodope: From mesozoic convergence to cenozoic extension. Review of petro-structural data in the geochronological frame. In: E. Skourtsos and Gordon S. Lister (Eds.), The Geology of Greece, Journal of the Virtual Explorer, Electronic Edition, ISSN 1441–8142, Volume 42, Paper 1.
Cabri, L.J., 1981. Platinum-group elements: mineralogy, geology, recovery. Published for the Geology division of CIM by the Canadian Institute of Mining and Metallurgy.
Cabri, L.J., 1965. Phase relations in the Au-Ag-Te system and their mineralogical significance. Econ. Geol. 60, 1569–1606.
Cabri, L.J., Harris, D.C., 1973. Michenerite (PdBiTe) redefined and froodite (PdBi 2) confirmed from the Sudbury area. Can. Mineral. 11, 903–912.
Ciobanu, C.L., Cook, N.J., Pring, A., 2005. Bismuth tellurides as gold scavengers. In: Mineral Deposit Research: Meeting the Global Challenge. Springer, pp. 1383–1386.
Ciobanu, C.L., Pring, A., Cook, N.J., Self, P., Jefferson, D., Dima, G.I., Melnikov, V., 2009. Chemical-structural modularity in the tetradymite group: a HRTEM study. Am. Mineral. 94, 517–534.
Cockerton, A.B.D., Tomkins, A.G., 2012. Insights into the liquid bismuth collector model through analysis of the Bi-Au Stormont skarn prospect, Northwest Tasmania. Econ. Geol. 107, 667–682. http://dx.doi.org/10.2113/econgeo.107.4.667.
Cook, N.J., Ciobanu, C.L., 2004. Bismuth tellurides and sulphosalts from the Larga hydrothermal system, Metaliferi Mts, Romania: paragenesis and genetic significance. Mineral. Mag. 68, 301–321. http://dx.doi.org/10.1180/0026461046820188.
Cook, N.J., Ciobanu, C.L., Wagner, T., Stanley, C.J., 2007. Minerals of the system Bi–Te–Se–S related to the tetradymite archetype: review of classification and compositional variation. Can. Mineral. 45, 665–708.
Dixon, J.E., Dimitriadis, S., 1984. Metamorphosed ophiolitic rocks from the Serbo-Macedonian Massif, near Lake Volvi, North-east Greece. Geol. Soc. Lond. Spec. Publ. 17, 603–618. http://dx.doi.org/10.1144/GSL.SP.1984.017.01.47.
Douglas, N., 2000. The liquid bismuth collector model: an alternative gold deposition mechanism. In: Geological Society of Australia Abstracts. Geological Society of Australia; 1999, p. 135.
Economou-Eliopoulos, M., 2010. Platinum-group elements(PGE)in various geotectonic settings: opportunities and risks. Hell. J. Geosci. 45 (45), 65–82.
Economou-Eliopoulos, M., 2005. Exploration for Deposits of Platinum-Group Elements. Mineral. Assoc. Canada Short Course 35 (35), 203–246.
Economou-Eliopoulos, M., Eliopoulos, D.G., 2000. Palladium, platinum and gold concentration in porphyry copper systems of Greece and their genetic significance. Ore Geol. Rev. 16, 59–70. http://dx.doi.org/10.1016/S0169-1368(99)00024-4.
Eldorado Gold Corp, 2017. Eldorado Gold Corporation - Assets - Resources and Reserves.
Eliopoulos, D., Economou-Eliopoulos, M., Zelyaskova-Panayiotova, M., 2014. Critical Factors Controlling Pd and Pt Potential in Porphyry Cu–Au Deposits: evidence from the Balkan Peninsula. Geosciences 4, 31–49. http://dx.doi.org/10.3390/geosciences4010031.
Eliopoulos, D.G., Economou-Eliopoulos, M., 1991. Platinum-group element and gold contents in the Skouries porphyry copper deposit, Chalkidiki Peninsula, northern Greece. Econ. Geol. 86, 740–749. http://dx.doi.org/10.2113/gsecongeo.86.4.740.
Frei, R., 1995. Evolution of Mineralizing Fluid in the Porphyry Copper System of the Skouries Deposit, Northeast Chalkidiki (Greece): Evidence from Combined Pb-Sr and Stable Isotope Data. Econ. Geol. 90, 746–762.
Frei, R., 1992. Isotope (Pb, Rb-Sr, S, O, C, U-Pb) geochemical investigations on Tertiary intrusives and related mineralizations in the Serbomacedonian Pb-Zn. Sb + Cu-Mo metallogenic province in Northern Greece, Swiss Federal Institute of Technology (ETH), Zurich.
Gather, B., Blachnik, R., 1974. Gold-Bismuth-Tellurium System. Z. Met. 65, 653–656.
Grundler, P.V., Brugger, J., Etschmann, B.E., Helm, L., Liu, W., Spry, P.G., Tian, Y., Testemale, D., Pring, A., 2013. Speciation of aqueous tellurium(IV) in hydrothermal solutions and vapors, and the role of oxidized tellurium species in Te transport and gold deposition. Geochim. Cosmochim. Acta 120, 298–325. http://dx.doi.org/10.1016/j.gca.2013.06.009.
Hahn, A., 2015. Nature, timing and geodynamic context of polymetallic mineralisation in the Kassandra mining district. Kingston University, North Greece.
Harangi, S., Downes, H., Thirlwall, M., Gméling, K., 2007. Geochemistry, petrogenesis and geodynamic relationships of miocene calc-alkaline volcanic rocks in the western Carpathian arc, Eastern Central Europe. J. Petrol. 48, 2261–2287. http://dx.doi.org/10.1093/petrology/egm059.
Harris, C.R., Pettke, T., Heinrich, C.A., Rosu, E., Woodland, S., Fry, B., 2013. Tethyan mantle metasomatism creates subduction geochemical signatures in non-arc Cu–Au–Te mineralizing magmas, Apuseni Mountains (Romania). Earth Planet. Sci. Lett. 366, 122–136. http://dx.doi.org/10.1016/j.epsl.2013.01.035.
Hein, K.A.A., Zaw, K., Mernagh, T.P., 2006. Linking mineral and fluid inclusion paragenetic studies: the Batman deposit, Mt. Todd (Yimuyn Manjerr) goldfield, Australia. Ore Geol. Rev. 28, 180–200. http://dx.doi.org/10.1016/j.oregeorev.2005.05.001.
Helmy, H.M., Ballhaus, C., Berndt, J., Bockrath, C., Wohlgemuth-Ueberwasser, C., 2007. Formation of Pt, Pd and Ni tellurides: Experiments in sulfide-telluride systems. Contrib. Mineral. Petrol. 153, 577–591. http://dx.doi.org/10.1007/s00410-006-0163-7.
Henley, R.W., Berger, B.R., 2013. Nature's refineries - metals and metalloids in arc volcanoes. Earth-Sci. Rev. 125, 146–170. http://dx.doi.org/10.1016/j.earscirev.2013.07.007.
Henley, R.W., Mavrogenes, J., Tanner, D., 2012. Sulfosalt melts and heavy metal (As-Sb-Bi-Sn-Pb-Tl) fractionation during volcanic gas expansion: the El Indio (Chile) paleofumarole. Geofluids 12, 199–215. http://dx.doi.org/10.1111/j.1468-8123.2011.00357.x.
Hoffman, E., Maclean, W.H., 1976. Phase relations of Michenerite and Merenskyite in the Pd-Bi-Te system. Econ. Geol. 71, 1461–1468.
Holwell, D.A., McDonald, I., 2010. A review of the behaviour of platinum group elements within natural magmatic sulfide ore systems. Platin. Met. Rev. 54, 26–36. http://dx.doi.org/10.1595/147106709X480913.
Jankovic, S., 1997. The Carpatho-Balkanides and adjacent area: a sector of the Tethyan Eurasian metallogenic belt. Miner. Depos. 32, 426–433. http://dx.doi.org/10.1007/s001260050110.
Jankovic, S., 1977. Metallogeny and Place Tectonics in the North-eastern Mediterranean.
Kalogeropoulos, S.I., Kilias, S.P., Bitzios, D.C., Nicolaou, M., Both, R.A., 1989. Genesis of the Olympias carbonate-hosted Pb-Zn(Au, Ag) sulfide ore deposit, eastern Chalkidiki Peninsula, northern Greece. Econ. Geol. 84, 1210–1234. http://dx.doi.org/10.2113/gsecongeo.84.5.1210.
Kehayov, R., Bogdanov, K., 1987. The fluid chemical evolution of the Elatsite porphyry Cu-Au-PGE deposit, Bulgaria. Petrology 1173–1176.
Kroll, T., Muller, D., Seifert, T., Herzig, P.M., Schneider, A., 2002. Petrology and geochemistry of the shoshonite-hosted Skouries porphyry Cu-Au deposit, Chalkidiki. Greece. Miner. Depos. 37, 137–144. http://dx.doi.org/10.1007/s00126-001-0235-6.
Lefort, D., Hanley, J., Guillong, M., 2011. Subepithermal Au-Pd mineralization associated with an alkalic porphyry Cu-Au deposit, Mount Milligan, Quesnel Terrane, British Columbia, Canada. Econ. Geol. 106, 781–808. http://dx.doi.org/10.2113/econgeo.106.5.781.
Maier, W.D., Bowen, M.P., 1996. The UG2-Merensky reef interval of the Bushveld Complex northwest of Pretoria. Miner. Depos. 31, 386–393.
Marchev, P., Kaiser-Rohrmeier, M., Heinrich, C., Ovtcharova, M., von Quadt, A., Raicheva, R., 2005. 2: Hydrothermal ore deposits related to post-orogenic extensional magmatism and core complex formation: the Rhodope Massif of Bulgaria and Greece. Ore Geol. Rev. 27, 53–89. http://dx.doi.org/10.1016/j.oregeorev.2005.07.027.
Markham, N.L., 1960. Synthetic and natural phases in the system Au-Ag-Te. Econ. Geol. 55, 1148–1178.
Mavrogenes, J., Henley, R.W., Reyes, A.G., Berger, B., 2010. Sulfosalt melts: evidence of high-temperature vapor transport of metals in the formation of high-sulfidation lode gold deposits. Econ. Geol. 105, 257–262. http://dx.doi.org/10.2113/gsecongeo.105.2.257.
McFall, K., Roberts, S., Naden, J., Wilkinson, C., Wilkinson, J., Boyce, A., 2017. Hydrothermal transport of PGEs in porphyry systems – a fluid history of the Skouries Cu–Au (PGE) porphyry deposit. Appl. Earth Sci. 1. http://dx.doi.org/10.1080/03717453.2017.1306277.
Micko, J.M., Tosdal, R.M.T., Bissig, T.B., Chamberlain, C.M.C., Simpson, K.A.S., 2014. Hydrothermal Alteration and Mineralization of the Galore Creek Alkalic Cu-Au Porphyry Deposit, Northwestern British Columbia, Canada. Econ. Geol. 891–914.
Mutschler, F.E., Griffen, M.E., Stevens, D.S., Shannon, S.S., 1985. Precious metal deposits related to alkaline rocks in the North American Cordillera; an interpretive review. S. Afr. J. Geol. 88, 355 LP– 377.
Okamoto, H., Massalski, T.B., 1983. The Au − Bi (Gold-Bismuth) system. Bull. Alloy Phase Diagrams 4, 401–407. http://dx.doi.org/10.1007/BF02868093.
Pašava, J., Vymazalová, A., Košler, J., Koneev, R.I., Jukov, A.V., Khalmatov, R.A., 2010. Platinum-group elements in ores from the Kalmakyr porphyry Cu-Au-Mo deposit, Uzbekistan: bulk geochemical and laser ablation ICP-MS data. Miner. Depos. 45, 411–418. http://dx.doi.org/10.1007/s00126-010-0286-7.
Pass, H.E., Cooke, D.R., Davidson, G., Maas, R., Dipple, G., Rees, C., Ferreira, L., Taylor, C., Deyell, C.L., 2014. Isotope geochemistry of the Northeast zone, Mount Polley alkalic Cu-Au-Ag porphyry deposit, British Columbia: a case for carbonate assimilation. Econ. Geol. 109, 859–890.
Piercey, S.J., 2014. Modern Analytical Facilities 2. A review of quality assurance and quality control (QA/QC) procedures for lithogeochemical data. Geosci. Canada 41, 75–88.
Piestrzynski, A., 1994. Pd-minerals in the Santo Tomas II porphyry copper deposit, Tuba, Benguet, Philippines. Miner. Pol. 25, 21–31.
Plotinskaya, O.Y., Azovskova, O.B., Abramov, S.S., Groznova, E.O., Novoselov, K.A., Seltmann, R., Spratt, J., 2018. Precious metals assemblages at the Mikheevskoe porphyry copper deposit (South Urals, Russia) as proxies of epithermal overprinting. Ore Geol. Rev 10.1016/j.oregeorev.2018.01.025.
Prichard, H.M., Knight, R.D., Fisher, P.C., McDonald, I., Zhou, M.F., Wang, C.Y., 2013. Distribution of platinum-group elements in magmatic and altered ores in the Jinchuan intrusion, China: an example of selenium remobilization by postmagmatic fluids. Miner. Depos. 48, 767–786. http://dx.doi.org/10.1007/s00126-013-0454-7.
Richards, J.P., 2015. Tectonic, magmatic, and metallogenic evolution of the Tethyan orogen: from subduction to collision. Ore Geol. Rev. 70, 323–345. http://dx.doi.org/10.1016/j.oregeorev.2014.11.009.
Richards, J.P., 2014. Porphyry and Related Deposits in Subduction and Post-Subduction Settings 88, 535–537.
Rosu, E., Seghedi, I., Downes, H., Alderton, D., Szakacs, A., Pecskay, Z., Panaiotu, C., Panaiotu, C., Nedelcu, L., 2005. Extension-related Miocene calc-alkaline magmatism in the Apuseni Mountains, Romania: origin of magmas. Schweizerische Mineral. Petrogr. Mitteilungen 83, 153–172.
Scholten, L., Watenphul, A., Beermann, O., Testemale, D., Ames, D., Schmidt, C., 2018. Nickel and platinum in high-temperature H 2 O + HCl fluids: implications for hydrothermal mobilization. Geochim. Cosmochim. Acta 224, 187–199. http://dx.doi.org/10.1016/j.gca.2018.01.005.
Sillitoe, R.H., 2010. Porphyry copper systems. Econ. Geol. 105, 3–41. http://dx.doi.org/10.2113/gsecongeo.105.1.3.
Siron, C.R., Rhys, D., Thompson, J.F.H., Baker, T., Veligrakis, T., Camacho, A., Dalampiras, L., 2018. Structural controls on porphyry Au-Cu and Au-rich polymetallic Carbonate-hosted replacement deposits of the Kassandra mining District, Northern Greece. Econ. Geol. 113, 309–345. http://dx.doi.org/10.5382/econgeo.2018.4552.
Siron, C.R., Thompson, J.F.H., Baker, T., Friedman, R., Tsitsanis, P., Russell, S., Randall, S., Mortensen, J., 2016. Chapter 2 Magmatic and Metallogenic Framework of Au-Cu

Porphyry and Polymetallic Carbonate- Hosted Replacement Deposits of the Kassandra Mining District , Northern Greece. Econ. Geol. Spec. Publ. 19, 29–55.
Sotnikov, V.I., Berzina, A.N., Economou-Eliopoulos, M., Eliopoulos, D.G., 2001. Palladium, platinum and gold distribution in porphyry Cu - Mo deposits of Russia and Mongolia. Ore Geol. Rev. 18, 95–111. http://dx.doi.org/10.1016/S0169-1368(01)00018-X.
Steele, T.W., 1978. A guide to the reporting of analytical results relating to the certification of geological reference materials. Geostand. Geoanalytical Res. 2, 31–33.
Tarkian, M., Eliopoulos, D.G., Economou-Eliopoulos, M., 1991. Mineralogy of precious metals in the skouries porphyry copper-deposit, Northern Greece. Neues Jahrb. Fur Mineral. 529–537.
Tarkian, M., Hünken, U., Tokmakchieva, M., Bogdanov, K., 2003. Precious-metal distribution and fluid-inclusion petrography of the Elatsite porphyry copper deposit, Bulgaria. Miner. Depos. 38, 261–281. http://dx.doi.org/10.1007/s00126-002-0336-x.
Tarkian, M., Koopmann, G., 1995. Platinum-group minerals in the Santo Tomas II (Philex) porphyry copper-gold deposit, Luzon Island, Philippines. Miner. Depos. 30, 39–47. http://dx.doi.org/10.1007/BF00208875.
Tarkian, M., Stribrny, B., 1999. Platinum-group elements in porphyry copper deposits: a reconnaissance study. Mineral. Petrol. 65, 161–183. http://dx.doi.org/10.1007/BF01161959.
Thompson, J.F.H., Lang, J.R., Stanley, C.R., 2001. Platinum group elements in alkaline porphyry deposits, British Columbia. Explor. Min. Br. Columbia Mines Branch Part B 57–64.
Tooth, B., Brugger, J., Ciobanu, C., Liu, W., 2008. Modeling of gold scavenging by bismuth melts coexisting with hydrothermal fluids. Geology 36, 815–818. http://dx.doi.org/10.1130/G25093A.1.
Tooth, B., Ciobanu, C.L., Green, L., O'Neill, B., Brugger, J., 2011. Bi-melt formation and gold scavenging from hydrothermal fluids: An experimental study. Geochim. Cosmochim. Acta 75, 5423–5443.
Voronin, M.V., Osadchii, E.G., Brichkina, E.A., 2017. Thermochemical properties of silver tellurides including empressite (AgTe) and phase diagrams for Ag–Te and Ag–Te–O. Phys. Chem. Miner. 44, 639–653. http://dx.doi.org/10.1007/s00269-017-0889-y.
Voudouris, P.C., Melfos, V., Spry, P.G., Kartal, T., Schleicher, H., Moritz, R., Ortelli, M., 2013. The Pagoni Rachi/Kirki Cu-Mo ± Re ± Au deposit, northern Greece: Mineralogical and fluid inclusion constraints on the evolution of a telescoped porphyry-epithermal system. Can. Mineral. 51, 253–284. http://dx.doi.org/10.3749/canmin.51.2.253.
Vymazalová, A., Laufek, F., Kristavchuk, A.V., Chareev, D.A., Drábek, M., 2015. The system Ag–Pd–Te: phase relations and mineral assemblages. Mineral. Mag. 79, 1813–1832. http://dx.doi.org/10.1180/minmag.2015.079.7.11.
Wagner, T., 2007. Thermodynamic modeling of Au-Bi-Te melt precipitation from high-temperature hydrothermal fluids: preliminary results. Digging Deep. Vols 1 2 Digging Deep. 769–772.
Wang, M., Gutzmer, J., Michalak, P.P., Guo, X., Xiao, F., Wang, W., Liu, K., 2014. PGE geochemistry of the Fengshan porphyry–skarn Cu–Mo deposit, Hubei Province, Eastern China. Ore Geol. Rev. 56, 1–12. http://dx.doi.org/10.1016/j.oregeorev.2013.07.006.
Watterson, J.R., Gott, G.B., Neuerburg, G.J., Lakin, H.W., Cathrall, J.B., 1977. Tellurium, a guide to mineral deposits. J. Geochem. Explor. 8, 31–48. http://dx.doi.org/10.1016/0375-6742(77)90042-5.
Wilkinson, J.J., 2001. Fluid inclusions in hydrothermal ore deposits. Lithos 55, 229–272.
Wilson, A.J., Cooke, D.R., Harper, B.L., 2003. The Ridgeway gold-copper deposit: A high-grade alkalic porphyry deposit in the Lachlan fold belt, New South Wales, Australia. Econ. Geol. 98, 1637–1666. http://dx.doi.org/10.2113/gsecongeo.98.8.1637.
Xiong, Y., Wood, S.A., 2000. Experimental quantification of hydrothermal solubility of platinum-group elements with special reference to porphyry copper environments. Mineral. Petrol. 68, 1–28. http://dx.doi.org/10.1007/s007100050001.